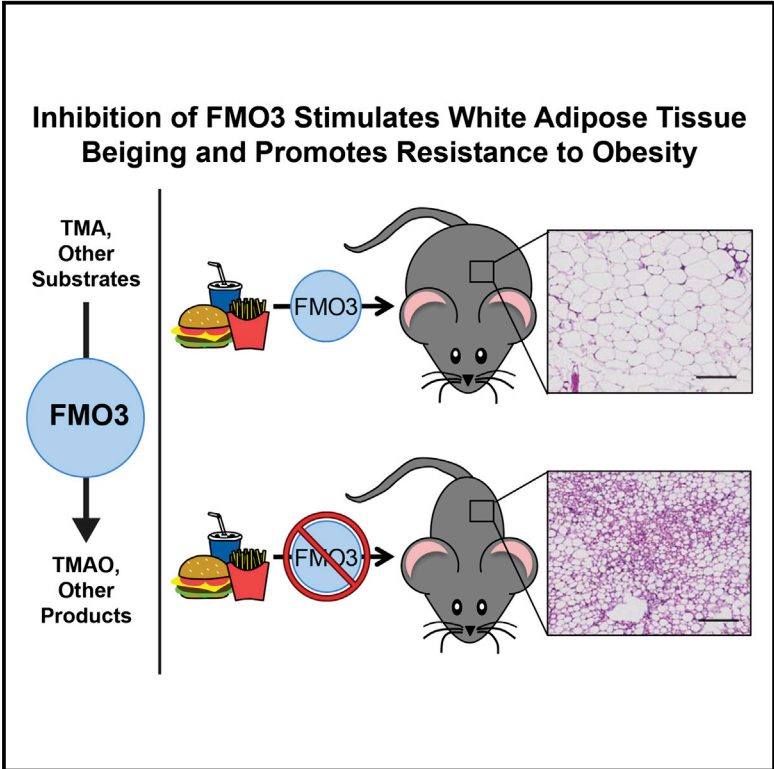


The TMAO-Producing Enzyme Flavin-Containing Monooxygenase 3 Regulates Obesity and the Beiging of White Adipose Tissue

Graphical Abstract



Authors

Rebecca C. Schugar, Diana M. Shih, Manya Warriar, ..., Aldons J. Lusis, Stanley L. Hazen, J. Mark Brown

Correspondence

brownm5@ccf.org

In Brief

Microbes resident in the human intestine represent a key transmissible environmental factor contributing to obesity and related disorders. Schugar et al. now show that expression of the TMAO-producing enzyme FMO3 is linked to obesity and energy expenditure in both mice and humans.

Highlights

- Plasma TMAO levels are elevated in type 2 diabetic patients
- Levels of the TMAO-producing enzyme FMO3 in adipose tissue correlate with obesity
- Pharmacologic and genetic inhibition of *Fmo3* stimulates white adipose tissue beiging
- Inhibition of *Fmo3* promotes resistance to obesity



The TMAO-Producing Enzyme Flavin-Containing Monooxygenase 3 Regulates Obesity and the Beiging of White Adipose Tissue

Rebecca C. Schugar,^{1,14,16} Diana M. Shih,^{13,16} Manya Warriar,^{1,14} Robert N. Helsley,^{1,14} Amy Burrows,^{1,14} Daniel Ferguson,^{1,14} Amanda L. Brown,^{1,14} Anthony D. Gromovsky,^{1,14} Markus Heine,¹² Arunachal Chatterjee,⁴ Lin Li,^{1,14} Xinmin S. Li,^{1,14} Zeneng Wang,^{1,14} Belinda Willard,^{1,14} YongHong Meng,¹³ Hanjun Kim,¹³ Nam Che,¹³ Calvin Pan,¹³ Richard G. Lee,⁸ Rosanne M. Crooke,⁸ Mark J. Graham,⁸ Richard E. Morton,¹ Carl D. Langefeld,⁵ Swapan K. Das,⁶ Lawrence L. Rudel,⁷ Nizar Zein,² Arthur J. McCullough,² Srinivasan Dasarathy,³ W.H. Wilson Tang,^{1,14,15} Bernadette O. Erokwu,¹¹ Chris A. Flask,¹¹ Markku Laakso,⁹ Mete Civelek,¹⁰ Sathyamangla V. Naga Prasad,⁴ Joerg Heeren,¹² Aldons J. Lulis,¹³ Stanley L. Hazen,^{1,14,15} and J. Mark Brown^{1,14,17,*}

¹Department of Cellular and Molecular Medicine, Cleveland Clinic, Cleveland, OH 44195, USA

²Department of Gastroenterology and Hepatology, Cleveland Clinic, Cleveland, OH 44195, USA

³Department of Pathobiology, Cleveland Clinic, Cleveland, OH 44195, USA

⁴Department of Molecular Cardiology, Cleveland Clinic, Cleveland, OH 44195, USA

⁵Department of Biostatistical Sciences, Wake Forest University School of Medicine, Winston-Salem, NC 27157-1040, USA

⁶Department of Endocrinology and Metabolism, Wake Forest University School of Medicine, Winston-Salem, NC 27157-1040, USA

⁷Department of Internal Medicine, Section on Molecular Medicine, Wake Forest University School of Medicine, Winston-Salem, NC 27157-1040, USA

⁸Cardiovascular Group, Antisense Drug Discovery, Ionis Pharmaceuticals, Inc., Carlsbad, CA 92010, USA

⁹Institute of Clinical Medicine, Internal Medicine, University of Eastern Finland and Kuopio University Hospital, 70210 Kuopio, Finland

¹⁰Department of Biomedical Engineering, University of Virginia, Charlottesville, VA 22904, USA

¹¹Departments of Radiology, Biomedical Engineering, and Pediatrics, Case Western Reserve University, Cleveland, OH 44195, USA

¹²Department of Biochemistry and Molecular Cell Biology, University Medical Center Hamburg-Eppendorf, Martinistraße 52, 20246 Hamburg, Germany

¹³Departments of Medicine, Microbiology, and Human Genetics, University of California, Los Angeles, Los Angeles, CA 90095, USA

¹⁴Center for Microbiome and Human Health, Cleveland Clinic, Cleveland, OH 44195, USA

¹⁵Department of Cardiovascular Medicine, Cleveland Clinic, Cleveland, OH 44195, USA

¹⁶These authors contributed equally

¹⁷Lead Contact

*Correspondence: brownm5@ccf.org

<http://dx.doi.org/10.1016/j.celrep.2017.05.077>

SUMMARY

Emerging evidence suggests that microbes resident in the human intestine represent a key environmental factor contributing to obesity-associated disorders. Here, we demonstrate that the gut microbiota-initiated trimethylamine N-oxide (TMAO)-generating pathway is linked to obesity and energy metabolism. In multiple clinical cohorts, systemic levels of TMAO were observed to strongly associate with type 2 diabetes. In addition, circulating TMAO levels were associated with obesity traits in the different inbred strains represented in the Hybrid Mouse Diversity Panel. Further, antisense oligonucleotide-mediated knockdown or genetic deletion of the TMAO-producing enzyme flavin-containing monooxygenase 3 (FMO3) conferred protection against obesity in mice. Complimentary mouse and human studies indicate a negative regulatory role for FMO3 in the beiging of white adipose tissue. Collectively, our studies reveal a link between the TMAO-producing

enzyme FMO3 and obesity and the beiging of white adipose tissue.

INTRODUCTION

There is strong evidence that microbes resident in the human intestine represent a key environmental factor contributing to obesity and associated insulin resistance (Bäckhed et al., 2004; Ley et al., 2005; Turnbaugh and Gordon, 2009; Cox et al., 2014). However, the molecular mechanisms by which gut microbiota promote obesity and insulin resistance in humans are incompletely understood. Recently, several independent groups have identified the gut microbiota-initiated trimethylamine (TMA)/flavin-containing monooxygenase 3 (FMO3)/trimethylamine N-oxide (TMAO) pathway as a potential modulator of cardiometabolic phenotypes in the host (Wang et al., 2011; Warriar et al., 2015; Miao et al., 2015; Shih et al., 2015), although our mechanistic understanding of this meta-organismal pathway is still incomplete. The TMA/FMO3/TMAO pathway is a microbe-to-host endocrine axis by which gut microbial metabolism of nutrients common in Western diets (phosphatidylcholine, choline, and L-carnitine) results in the production of the metabolite TMA,

which is exclusively generated by certain communities of gut microbiota (Wang et al., 2011; Koeth et al., 2013; Gregory et al., 2015; Romano et al., 2015). Then, the host hepatic enzyme flavin-containing monooxygenase 3 (FMO3) further metabolizes gut microbe-derived TMA to produce TMAO (Wang et al., 2011; Bennett et al., 2013). Importantly, the end product of this meta-organismal nutrient metabolism pathway, TMAO, is both a prognostic biomarker and mechanistically linked to cardiovascular disease (CVD) pathogenesis in humans (Wang et al., 2011, 2014, 2015; Koeth et al., 2013, 2014; Tang et al., 2013, 2014; Suzuki et al., 2016; Missailidis et al., 2016; Mafune et al., 2016; Trøseid et al., 2015; Zhu et al., 2016). Given the strong link between gut microbiota and both obesity and obesity-related disease in humans, and the links between the TMAO pathway and cardiometabolic diseases, we hypothesized that the TMAO pathway may be mechanistically linked to the pathogenesis of obesity. Here, we show that both antisense oligonucleotide-mediated knockdown and genetic deletion of the TMAO-producing enzyme FMO3 protect mice against high-fat diet-induced obesity, in part by stimulating the beiging of white adipose tissue, which may reduce the adverse effects of increased adiposity and improve overall metabolic health (Bartelt and Heeren, 2014). Collectively, our studies have uncovered a link between the gut microbe-driven TMA/FMO3/TMAO pathway and adipose tissue function.

RESULTS

Elevated Systemic Levels of TMAO Are Associated with Type 2 Diabetes in Humans

To first establish clinical relevance, we investigated the relationship of fasting plasma levels of choline or TMAO with type 2 diabetes mellitus (T2DM) risk in two independent cohorts of subjects undergoing elective cardiac risk factor evaluation and recommendations in our preventative cardiology clinic ($n = 187$) or evaluation for suspected non-alcoholic fatty liver disease in our hepatology clinic ($n = 248$). Patient demographics, laboratory values, and clinical characteristics for both cohorts ($n = 435$ combined) are provided in Tables S1–S3. Plasma concentrations of TMAO were significantly higher in subjects with T2DM in each of the individual cohorts and when the cohorts were combined (Figure 1A). Fasting choline levels were significantly higher only in T2DM subjects from the hepatology cohort (Figure 1B). Similarly, we observed a dose-dependent association between higher TMAO concentrations and the presence of T2DM (Figure 1C), while the association between choline and T2DM was seen only in the hepatology cohort (Figure 1D). After adjustments for multiple comorbidities, prevalent CVD and CVD risk factors, medications, and renal function, TMAO remained a strong predictor of T2DM risk in both cohorts analyzed alone, as well as when the cohorts were combined (Figure S1). Collectively, these data suggest that circulating levels of the meta-organismal metabolite TMAO are closely correlated with T2DM risk in humans.

Plasma TMAO Levels in Mice and FMO3 mRNA Expression in Men Demonstrate Positive Correlations with Obesity

First, using a systems genetics approach in mice, we examined various obesity-related traits and circulating TMAO levels in mice

from the Hybrid Mouse Diversity Panel (HMDP) fed an obesogenic high-fat and high-sucrose diet (Parks et al., 2013). Across the different inbred strains represented in the Hybrid Mouse Diversity Panel, circulating levels of TMAO were positively associated with body weight, fat mass, mesenteric adiposity, and subcutaneous adiposity (Figures 2A–2D). Given the observed associations between TMAO and obesity across the diverse inbred strains of mice, we next set out to determine whether expression of *FMO3*, which encodes the TMAO-producing enzyme, was differentially expressed in the adipose tissue of overweight or obese humans. To do this, we first examined a random sampling ($n = 770$) of a large population-based study of Finnish men known as the METSIM study (Stancáková et al., 2009). This study performed dense phenotypic characterization of subjects for characteristics related to adiposity and insulin sensitivity, including adipose biopsies and microarray expression analysis (Stancáková et al., 2009; Civelek et al., 2017). When we examined the correlation between expression levels of all members of the FMO family in adipose tissue with metabolic traits in this population, we found that *FMO3* was positively correlated with body mass index (BMI) and waist-to-hip ratio and negatively correlated with the Matsuda Index (Matsuda and DeFronzo, 1999), which is a measure of insulin sensitivity (Figure 2E). Interestingly, *FMO3* mRNA expression levels in human adipose tissue were significantly negatively correlated with several genes that represent selective markers of beige or brown adipocytes that have recently been reported (Wu et al., 2012; Uszar et al., 2014) (Figure 2E). These data suggest that *FMO3* expression is negatively associated with beiging signatures in human subcutaneous white adipose tissue.

Given that the METSIM study only includes Finnish men, we set out to validate microarray expression data in several distinct cohorts spanning both men and women of European American and African American ethnicity. Importantly, these validation cohorts were also chosen for their gender, ethnic and racial diversity, and because each has been extensively characterized for obesity and cardiometabolic phenotypes (Das et al., 2015; Sharma et al., 2016). The first cohort included 99 white, non-Hispanic Americans (42 males and 57 females) (Das et al., 2015). The second cohort included 260 African Americans (139 males and 121 females) (Sharma et al., 2016). In agreement with findings from the METSIM study (Figure 2E), we found that *FMO3* was positively correlated with BMI and adiposity and negatively correlated with insulin sensitivity in both European American and African American men and women (Figure S2). Also, the primary transcript variant of *FMO3* was negatively correlated with the beige/brown marker genes uncoupling protein 1 (*UCP1*) and PR domain-containing 16 (*PRDM16*) (Figure S2).

In separate studies, we sought to examine whether similar associations were observed between *FMO3* expression in human liver and metabolic traits using liver biopsies from obese patients undergoing bariatric surgery and normal weight controls. In contrast to our findings in human adipose tissue (Figures 2E and S2), we did not find significant correlations between liver *FMO3* protein levels and metabolic traits in this cohort (Figure S3). Of note, the protein expression of *FMO3* in human liver does not significantly differ between males and females in the cohort under study ($n = 15$ males, $n = 35$ females; $p = 0.79$) (Figure S3).

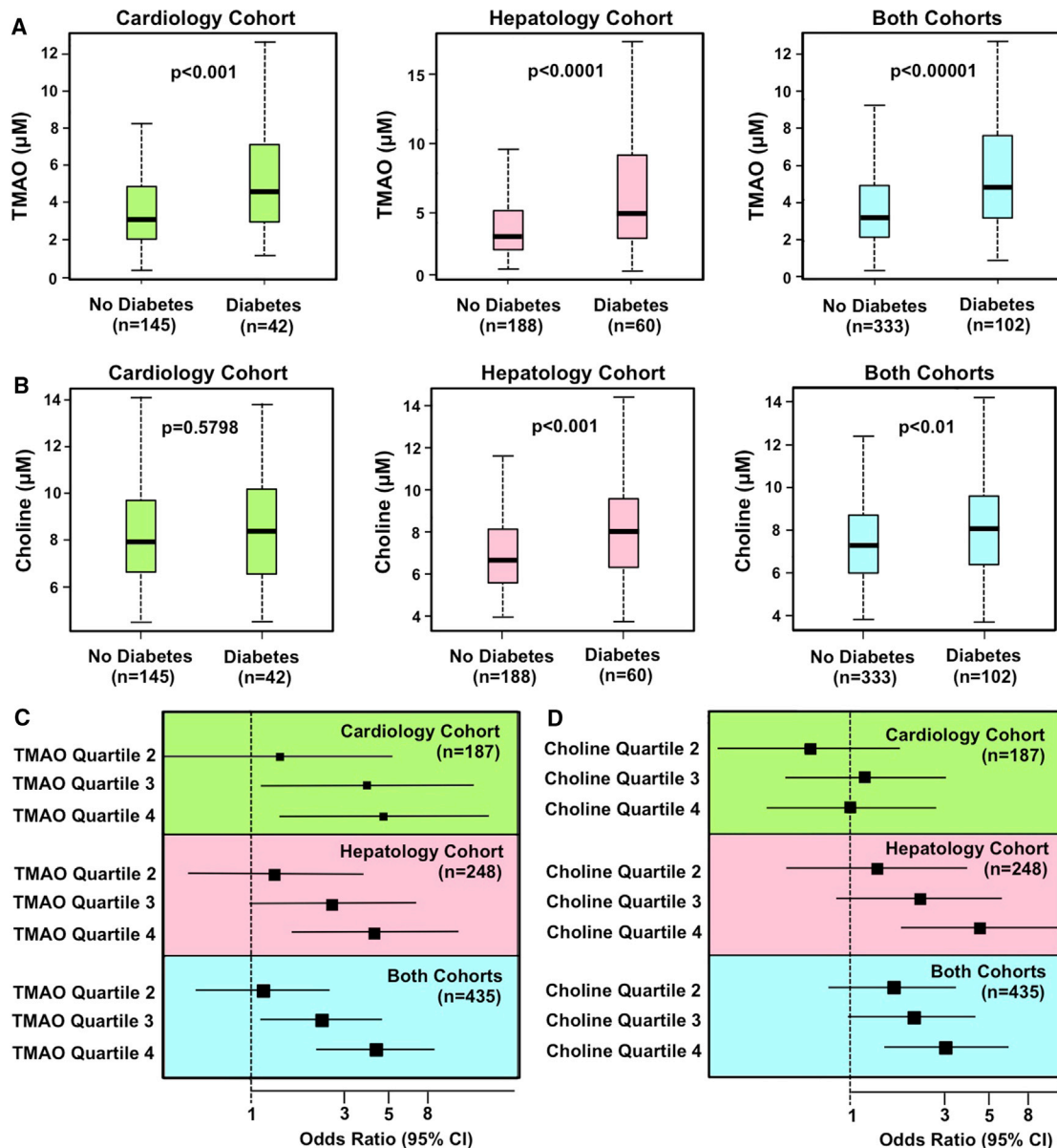


Figure 1. Elevated Circulating Levels of TMAO Are Associated with Type 2 Diabetes Mellitus in Humans

We recruited two separate cohorts of stable subjects in preventative cardiology ($n = 187$) or hepatology clinics ($n = 248$) to evaluate the association between fasting circulating choline or trimethylamine N-oxide (TMAO) levels and prevalent type 2 diabetes (T2DM). The total number of subjects recruited in both studies was 435. Patient demographics, laboratory values, and clinical characteristics are provided in [Tables S1–S3](#) and [Figure S1](#).

(A) Relationship of fasting plasma TMAO concentrations and prevalent T2DM. Boxes represent the 25th, 50th, and 75th percentiles of plasma TMAO concentration, and whiskers represent the 10th and 90th percentiles.

(B) Relationship between fasting plasma choline concentrations and prevalent T2DM. Boxes represent the 25th, 50th, and 75th percentiles of plasma choline concentration, and whiskers represent the 10th and 90th percentiles.

(C) Forest plots of the odds ratio of prevalent T2DM and quartiles of TMAO; bars represent 95% confidence intervals.

(D) Forest plots of the odds ratio of prevalent T2DM and quartile of choline; bars represent 95% confidence intervals.

Knockdown of FMO3 Protects Mice from High-Fat Diet-Induced Obesity by Stimulating the Beiging of White Adipose Tissue

To further examine the potential of the meta-organismal TMAO pathway to impact obesity, we utilized a second-generation antisense oligonucleotide (ASO) to inhibit the expression of *Fmo3* in

mice challenged with a high-fat diet (HFD) ([Figure 3](#)). *Fmo3* ASO treatment resulted in >90% knockdown of *Fmo3* mRNA levels in mouse liver in both chow-fed and high-fat diet-fed mice ([Figure 3A](#)). In line with this, FMO3 knockdown caused accumulation of the FMO3 substrate TMA in mice on both diets, while reductions in its product, TMAO, were seen only in chow-fed mice

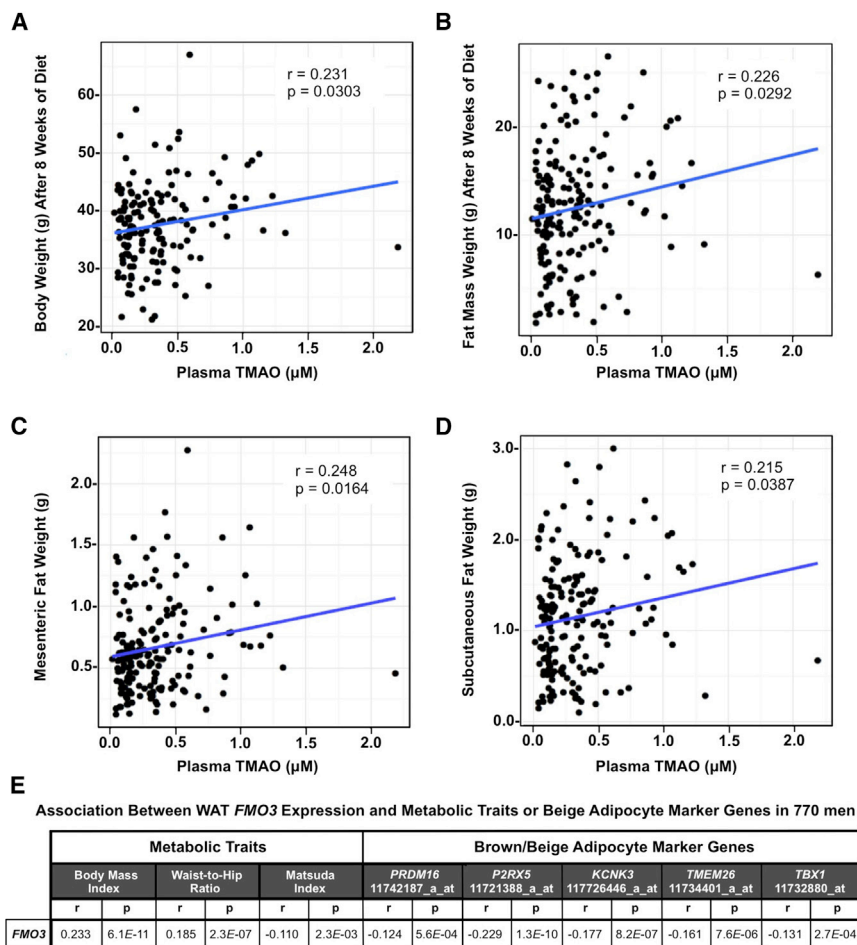


Figure 2. Plasma TMAO Levels in Mice and *FMO3* mRNA Expression in Men Demonstrate Positive Correlations with Obesity

(A–D) Correlation of plasma trimethylamine N-oxide (TMAO) levels with obesity-related traits in 180 male mice from 92 inbred strains within the Hybrid Mouse Diversity Panel (HMDP) after 8-week feeding of a high-fat and high-sucrose diet. Correlation coefficient (r) and p value (p) are indicated for each obesity trait. (A) Correlation between plasma TMAO and body weight. (B) Correlation between plasma TMAO and fat mass. (C) Correlation between plasma TMAO and mesenteric fat weight. (D) Correlation between plasma TMAO and subcutaneous fat weight. (E) Correlations between human white adipose tissue flavin monooxygenase 3 (*FMO3*) mRNA expression and metabolic traits or brown/beige adipocyte marker gene expression ($n = 770$). The gene name and probe set ID is provided for each of the brown/beige adipocyte marker genes.

(Figures 3B and 3C). Indeed, the overall lower TMAO levels in the high-fat diet groups may be due to less overall choline substrate in the high-fat diet (Table S4). Despite documenting comparable food intake on high-fat diet (Figure S4D), *FMO3* knockdown resulted in significantly decreased body weight gain (Figure 3D). The attenuation in body weight gain observed appeared to be largely attributed to decreased white adipose tissue weight (Figure 3E), with magnetic resonance imaging (Figure 3F) demonstrating that both peritoneal (Figure 3G) and subcutaneous (Figure 3H) adipose tissue mass were markedly reduced with *Fmo3* ASO treatment. Collectively, *Fmo3* ASO treatment altered body composition, reducing the overall percentage of fat mass (Figure 3I), while increasing the percent of lean mass (Figure 3J) in the high-fat diet-fed cohort. In additional studies, gonadal white adipose tissue *Fmo3* mRNA levels were observed to be $\sim 1,000$ -fold lower than hepatic *Fmo3* mRNA levels (Figure S4A). Importantly, *Fmo3* ASO treatment protected against high-fat diet-induced obesity in both female (Figure 3) and male (Figure S4B) mice, despite sexual dimorphism in total FMO activity in liver and gonadal white adipose tissue (Figure S4C).

Given the fact that *FMO3* expression was negatively correlated with brown and beige adipocyte gene markers in human adipose tissue (Figure 2E), we next examined the effect of

uncoupling protein 1 (*Ucp1*), and a 3-fold increase in transmembrane protein 26 (*Tmem26*) (Figure 4B). In parallel, plasma membrane-associated $\beta 1$ -AR abundance was increased 4.7-fold in *Fmo3* ASO-treated mice (Figure 4C), which was associated with a 3-fold increase in cyclic AMP levels in gonadal adipose tissue (Figure 4D). To examine the role of *FMO3* in cold-induced transcriptional reprogramming, we housed mice in either room temperature (22°C) or cold (4°C) conditions. Interestingly, the normal cold-induced upregulation of the thermogenic transcriptional regulator peroxisome proliferator-activated receptor gamma coactivator 1-alpha (*Ppargc1a*) (Puigserver et al., 1998) was much higher in mice treated with *Fmo3* ASO in multiple adipose depots (Figure 4E).

We next investigated the physiological role of *FMO3* in cold-induced thermogenic reprogramming by performing indirect calorimetry in high-fat diet-fed *Fmo3* ASO-treated mice housed at thermoneutrality (30°C), room temperature (22°C), or under cold stress (4°C). *FMO3* knockdown increased oxygen consumption (VO_2) and heat production under all temperature conditions (Figures 4F and 4G). Interestingly, the normal cold-induced increase in VO_2 and heat seen in control mice was significantly enhanced in the *Fmo3* ASO-treated mice housed at 4°C (Figures 4F and 4G). It is well documented that the

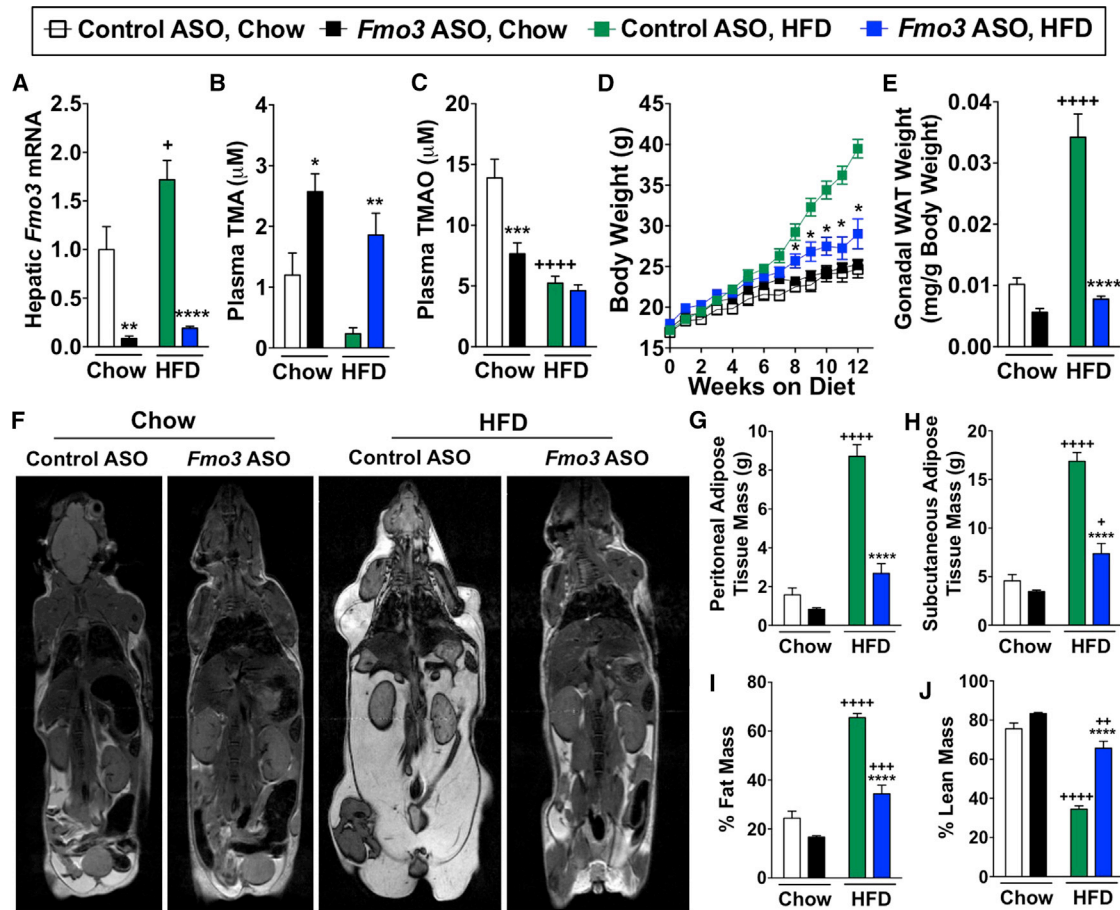


Figure 3. FMO3 Knockdown Protects Mice from High-Fat Diet-Induced Obesity by Stimulating the Beiging of White Adipose Tissue

At 6–8 weeks of age, female C57BL/6 mice were treated with either a non-targeting control ASO or *Fmo3* ASO in conjunction with either standard rodent chow or high-fat diet (HFD) feeding for the indicated times.

(A) Hepatic *Fmo3* mRNA expression was quantified by qPCR after 10 weeks.

(B) Plasma levels of TMA after 6 weeks.

(C) Plasma levels of TMAO after 6 weeks.

(D) Body weight changes over 12 weeks.

(E) Gonadal white adipose tissue (WAT) weight at necropsy.

(F–J) MRI images and subsequent quantification of adiposity in control and *Fmo3* ASO-treated mice maintained on diets for 14 weeks. (F) MRI images of control and *Fmo3* ASO-treated mice. (G) Peritoneal adipose tissue mass. (H) Subcutaneous adipose tissue mass. (I) Fat mass (%). (J) Lean mass (%).

All data represent the mean \pm SEM for $n = 5$ –10 mice per group. * $p \leq 0.05$, ** $p \leq 0.01$, *** $p \leq 0.001$, **** $p \leq 0.0001$ versus control ASO-treated mice fed the same diet; + $p \leq 0.05$, ++ $p \leq 0.01$, +++ $p \leq 0.001$, ++++ $p \leq 0.0001$ versus chow-fed mice treated with the same ASO.

preferred macronutrient fuel source (carbohydrates versus fats) differs under fasted and fed states as well as during cold stress, and dysregulation of this metabolic flexibility is thought to be a key component of the metabolic syndrome (Muio, 2014). High-fat diet-fed *Fmo3* ASO-treated mice have a marked improvement in metabolic flexibility in response to feeding (during the dark cycle) and cold (Figure 4H). In fact, *Fmo3* ASO-treated mice have a slightly larger increase in glucose oxidation (indicated by increased respiratory exchange ratio) during the dark cycle at thermoneutrality, and this enhanced metabolic flexibility becomes much more striking at 22°C and 4°C (Figure 4H). These data suggest that FMO3 inhibition facilitates feeding-induced fuel switching (from fats to carbohydrates), especially

under conditions of cold stress. Collectively, these data suggest that knockdown of FMO3 increases energy expenditure and enhances metabolic flexibility under conditions of cold stress.

Given that TMAO levels were linked to adiposity across multiple strains of mice (Figure 2), we hypothesized that TMAO itself may be directly involved in regulating adiposity. Therefore, we set out to determine the involvement of TMAO in the adipose tissue phenotype seen with FMO3 knockdown. To achieve this, we provided TMAO as a dietary supplement as previously described (Warrier et al., 2015) to control and *Fmo3* ASO-treated mice maintained on high-fat diet. Dietary provision of TMAO effectively raised levels of TMAO in the circulation, liver, and white adipose tissue in control and *Fmo3* ASO-treated mice (Figures S4E

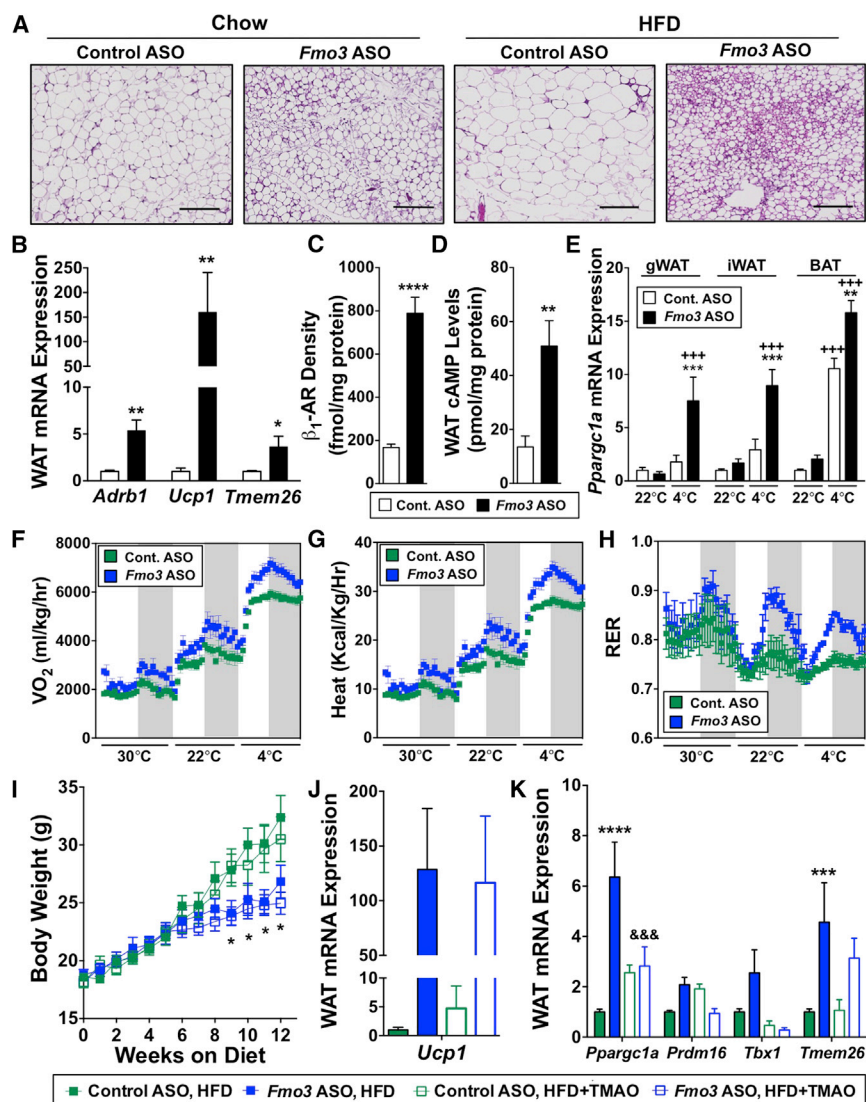


Figure 4. FMO3 Knockdown Stimulates the Beiging of White Adipose Tissue

(A–E) At 6–8 weeks of age, female C57BL/6 mice were treated with either a non-targeting control ASO or *Fmo3* ASO in conjunction with high-fat diet (HFD) feeding for 8–12 weeks. (A) Microscopic examination of H&E-stained gonadal white adipose tissue; scale bar represents 200 μ m. (B) Gonadal white adipose tissue (WAT) mRNA expression of β_1 -adrenergic receptor (*Adrb1*), uncoupling protein 1 (*Ucp1*), and transmembrane protein 26 (*Tmem26*) quantified by qPCR. (C) Surface density of β_1 -adrenergic receptor (β_1 -AR) in gonadal white adipose tissue quantified by radio-ligand binding assay. (D) Cyclic AMP (cAMP) levels in gonadal white adipose tissue. (E) Peroxisome proliferator-activated receptor gamma co-activator 1-alpha (*Ppargc1a*) mRNA expression was quantified by qPCR in gonadal (gWAT), inguinal (iWAT), and brown adipose tissue (BAT). (F–H) Mice were housed in metabolic cages for indirect calorimetry measurements. Gray background denotes dark cycle. (F) Oxygen consumption (VO_2). (G) Heat production. (H) Respiratory exchange ratio (RER).

(I–K) At 6–8 weeks of age, female C57BL/6 mice were treated with either a non-targeting control ASO or *Fmo3* ASO in conjunction with feeding of HFD or HFD supplemented with 0.02% w/w TMAO for 12 weeks. See also Figure S4.

(I) Body weight changes over 12 weeks. (J) Gonadal white adipose tissue (WAT) expression of uncoupling protein 1 (*Ucp1*).

(K) Gonadal white adipose tissue (WAT) expression of peroxisome proliferator-activated receptor gamma coactivator 1-alpha (*Ppargc1a*), PR domain-containing 16 (*Prdm16*), T-box transcription factor (*Tbx1*), and transmembrane protein 26 (*Tmem26*).

All data represent the mean \pm SEM for n = 5–10 mice per group. *p \leq 0.05, **p \leq 0.01, ***p \leq 0.001, ****p \leq 0.0001 versus control ASO-treated mice fed the same diet; +++p \leq 0.001 versus chow-fed mice treated with the same ASO; &&&p \leq 0.001 versus *Fmo3* ASO-treated mice fed an HFD.

and S4F). Interestingly, despite commensurate food consumption (Figure S4D), *Fmo3* ASO-treated mice had significantly lower plasma TMAO levels compared to control ASO-treated mice following dietary supplementation (Figure S4E). Importantly, dietary provision of TMAO did not reverse the ability of *Fmo3* ASO treatment to attenuate high-fat diet-induced body weight gain (Figure 4I). Likewise, dietary TMAO provision did not alter the ability of *Fmo3* ASO treatment to elevate *Ucp1* expression in gonadal white adipose tissue (Figure 4J). However, *Fmo3* ASO-driven increases in gonadal white adipose tissue genes involved in energy metabolism and the development of brown adipose tissue, including *Ppargc1a*, *Prdm16*, and T-box transcription factor (*Tbx1*) were reversed by dietary TMAO provision (Figure 4K). Collectively, these data demonstrate that provision of dietary TMAO can reverse a portion, but not all, of the transcriptional reorganization observed in white adipose tissue driven by FMO3 knockdown and suggest that future studies

should investigate the role of additional FMO3 products or substrates in energy metabolism.

Genetic Deletion of the TMAO-Producing Enzyme FMO3 Protects Mice from Obesity

To further examine the role of FMO3 in obesity, we examined global FMO3 knockout (*Fmo3*^{-/-}) mice generated using CRISPR-Cas9-mediated gene editing (Figure 5; Table S5). Hepatic FMO3 protein was undetectable by western blot in *Fmo3*^{-/-} mice (Figure 5A). In initial studies, we maintained *Fmo3*^{-/-} mice on a C57BL/6 background and fed a choline-supplemented chow-based diet. Under these non-obesogenic conditions, *Fmo3*^{-/-} mice accumulate plasma TMA and have diminished TMAO as predicted, and while there were no differences in food intake or body weight, they do exhibit significantly reduced adiposity compared to *Fmo3*^{+/+} mice (Figure 5B). To examine effects of FMO3 knockout on adiposity under

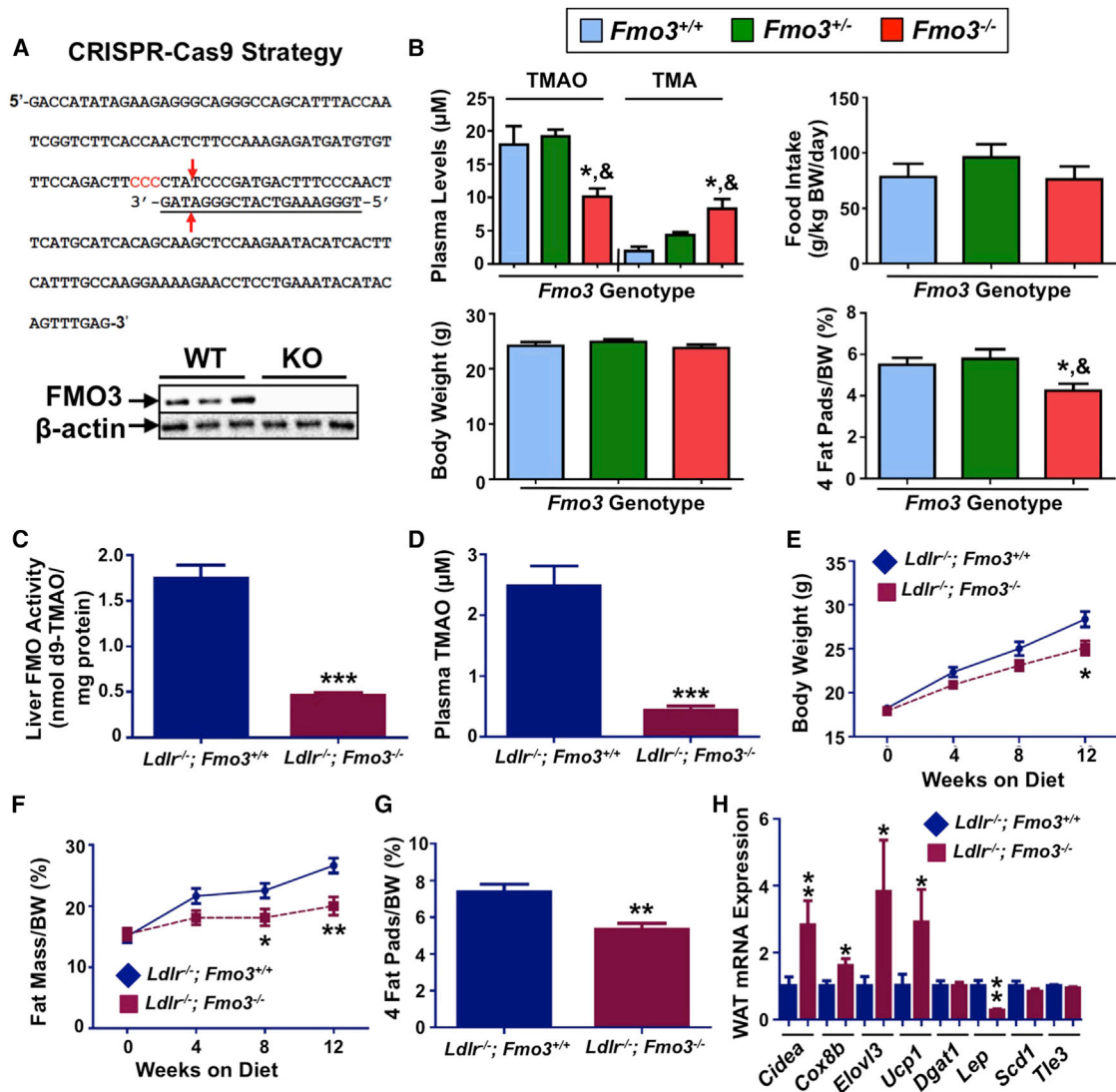


Figure 5. Genetic Deletion of FMO3 Protects Mice from Diet-Induced Obesity

(A) Top: CRISPR-Cas9 strategy for generating *Fmo3*^{-/-} mice. The sequence of exon 2 of the murine *Fmo3* coding sequence is shown. The target sequence (underlined) used for construction of the guide RNA is shown with arrows indicating predicted cleavage sites by Cas9. Bottom: immunoblotting analysis of FMO3 protein levels in the livers of wild-type (WT) and *Fmo3*^{-/-} (KO) mice.

(B) Decreased adiposity in *Fmo3*^{-/-} mice. *Fmo3*^{+/+} (n = 9), *Fmo3*^{+/-} (n = 6), and *Fmo3*^{-/-} (n = 11) mice were fed a 1.3% choline chloride (w/w) diet for 12 weeks before tissue collection. Plasma TMAO and TMA levels (top left), food intake (top right), body weight (bottom left), and four fat pads/body weight (%; bottom right) are shown. The four fat pads included in the four fat pads/body weight measurement were gonadal, mesentery, perirenal, and subcutaneous. *p ≤ 0.05 between *Fmo3*^{+/+} and *Fmo3*^{-/-} groups; &p ≤ 0.05 between *Fmo3*^{+/-} and *Fmo3*^{-/-} genotype groups.

(C–H) *Ldlr*^{-/-}; *Fmo3*^{-/-} mice are more resistant to obesity than *Ldlr*^{-/-} littermates when fed a Western diet for 12 weeks. (C) Liver FMO activity. (D) Plasma TMAO levels. (E) Body weight changes over 12 weeks. (F) Fat mass/body weight (%). (G) Four fat pads weight/body weight (%); the four fat pads measured were gonadal, mesentery, perirenal, and subcutaneous. (H) Gene expression analysis of subcutaneous fat pads of *Ldlr*^{-/-} (n = 17) and *Ldlr*^{-/-}; *Fmo3*^{-/-} (n = 9) mice. Cell death-inducing DFFA-like effector A (*Cidea*), cytochrome c oxidase subunit 8b (*Cox8b*), elongation of very long chain fatty acids protein 3 (*Elovl3*), uncoupling protein 1 (*Ucp1*), diglyceride acyltransferase 1 (*Dgat1*), leptin (*Lep*), stearyl coenzyme A (CoA) desaturase-1 (*Scd1*), transducin-like enhancer of split 3 (*Tle3*). *p ≤ 0.05, **p ≤ 0.01, and ***p ≤ 0.0001 between the two genotype groups.

obesogenic conditions we crossed *Fmo3*^{-/-} mice to the low-density lipoprotein knockout (*Ldlr*^{-/-}) background and maintained mice on a Western diet (Figures 5C–5H). Western diet-fed *Ldlr*^{-/-}; *Fmo3*^{-/-} mice had markedly reduced hepatic FMO activity (Figure 5C) and circulating TMAO levels (Figure 5D) when compared to *Ldlr*^{-/-}; *Fmo3*^{+/+} control mice. In agreement

with our studies in high-fat diet-fed *Fmo3* ASO-treated mice (Figures 3 and 4), Western-diet-fed *Ldlr*^{-/-}; *Fmo3*^{-/-} mice were protected against diet-induced obesity (Figures 5E–5G) and had increased expression of brown/beige adipocyte marker genes in the subcutaneous fat depots compared to *Ldlr*^{-/-}; *Fmo3*^{+/+} control mice (Figure 5H). Collectively, these data provide genetic

evidence that FMO3 is a negative regulator of beiging programs in white adipose tissue.

DISCUSSION

Obesity, insulin resistance, and atherosclerotic CVD are closely linked diseases that can be heavily impacted by the quantity and quality of dietary inputs. In a time where genetic and genomic approaches dominate clinical investigation, we are still constantly reminded that environmental factors such as diet can play a major role in disease pathogenesis. The meta-organismal TMAO pathway was initially discovered using untargeted metabolomics approaches to identify small molecules in plasma associated with CVD risk (Wang et al., 2011). In multiple follow-up studies, it has been shown that feeding atherosclerosis-prone mice diets enriched in either distinct nutrient precursors to TMA synthesis or TMAO itself enhances atherosclerotic CVD and thrombosis potential by altering host cholesterol metabolism and platelet hyper-reactivity (Koeth et al., 2013, 2014; Zhu et al., 2016). In parallel, ASO-mediated inhibition of the TMAO-producing enzyme FMO3 protects mice from atherosclerosis (Shih et al., 2015; Miao et al., 2015), possibly in part by stimulating an intestinal pathway of reverse cholesterol transport called transintestinal cholesterol excretion (TICE) and altering tissue sterol metabolism (Warrier et al., 2015; Shih et al., 2015). More recently, inhibition of the microbial enzymes responsible for generating TMA from choline, thereby reducing TMAO levels, was shown to similarly inhibit atherosclerosis in mice (Wang et al., 2015). Therefore, while significant mechanistic and clinical data indicate that the meta-organismal TMA/FMO3/TMAO pathway is closely linked to the pathogenesis of atherosclerosis in mice and humans (Brown and Hazen, 2015), here we provide evidence that the pathway can also impact the beiging of white adipose tissue. The key findings of the current study are that (1) circulating levels of the gut microbe-derived metabolite TMAO are associated with enhanced risk of T2DM in humans, (2) TMAO levels are associated with adiposity traits across mouse strains within the Hybrid Mouse Diversity Panel, (3) adipose tissue expression of *FMO3* is positively associated with obesity in humans, (4) *FMO3* mRNA expression is negatively associated with brown/beige adipocyte gene expression in white adipose tissue in humans, (5) *FMO3* knockdown or genetic deletion protects mice against high-fat diet-induced obesity, and (6) *FMO3* knockdown or genetic deletion is associated with the beiging of white adipose tissue in mice.

Although the vast majority of studies have focused on the TMA/FMO3/TMAO pathway in the context of CVD, several recent studies have linked this meta-organismal pathway to diabetes. In agreement with our findings here, several independent groups have found an association between circulating TMAO levels and both T2DM and the heightened adverse CVD outcomes in diabetics (Lever et al., 2014; Dambrova et al., 2016; Tang et al., 2017). Using a metabolomics platform, Miao and colleagues recently showed that mice with selective hepatic insulin resistance (liver insulin receptor knockout mice [LIRKO]) have elevated levels of circulating TMAO and a profound upregulation of the TMAO-producing enzyme FMO3 in the liver (Miao et al., 2015). This study also demonstrated that the hepatic expression

of FMO3 is suppressed by the postprandial hormone insulin yet is reciprocally stimulated by the fasting hormone glucagon (Miao et al., 2015). In addition to these findings in LIRKO mice, dietary supplementation with the FMO3 product TMAO is reported to exacerbate glucose intolerance in high-fat diet-fed mice (Gao et al., 2014). Collectively, a growing body of evidence suggests that the gut microbial TMAO pathway may be an attractive drug target for subjects with T2DM. Of note, while TMAO has been causally linked to atherosclerosis and thrombosis (Wang et al., 2011; Koeth et al., 2013; Zhu et al., 2016) and associated with obesity here, there is also literature that shows diets high in the TMAO source nutrient choline are associated with beneficial effects on fetal development and cognitive function in adults (Jiang et al., 2012; Shaw et al., 2009; Poly et al., 2011).

As drug discovery forges ahead, identifying the mechanisms driving the links among TMA, FMO3, TMAO, and human health and disease will be needed to understand where to therapeutically intervene. It is important to note that FMO3 is a promiscuous xenobiotic metabolizing enzyme with many substrates and products (Cashman and Zhang, 2006). In fact, FMO3 knockdown-associated effects on metabolic disease may be driven by factors other than TMA or TMAO. Although provision of supplemental TMAO reversed a subset of the *Fmo3* ASO-induced effects on adipose gene expression, it also makes clear that not all of the phenotypes observed by FMO3 knockdown are mediated by either TMA or TMAO. Additional work is needed to understand the most therapeutically tractable targets in the entire TMA/FMO3/TMAO meta-organismal pathway. Based on the present studies, it appears that the phenotypic effects of FMO3 knockdown or deletion could be driven by a combination of factors, including (1) chronic increases in the levels of TMA, (2) chronic decreases in the levels of TMAO, and/or (3) effects driven by other FMO3 substrates or products. It is interesting to note that dietary provision of TMAO reversed *Fmo3* ASO-driven increases in *Ppargc1a* but did not rescue *Fmo3* ASO-driven reductions in body weight or expression of *Ucp1* in white adipose tissue (Figures 5I–5K). Such findings support a model where TMAO may be involved in specific transcriptional reprogramming in adipocytes, but how TMAO is being sensed is still an unanswered question. TMA is known to activate the G-protein-coupled receptor trace amine-associated receptor 5 (TAAR5); however, TAAR5 does not recognize TMAO (Li et al., 2013). It will be important in future studies to determine whether TMA-driven activation of TAAR5 is coupled to metabolic reprogramming in the host and to identify potential host TMAO receptor(s). In conclusion, this work highlights a role for the TMA/FMO3/TMAO meta-organismal pathway in the progression of obesity-related disorders. Given the numerous strong associations of the gut microbe-driven TMAO pathway with human disease, this work has broad implications for drug discovery efforts targeting gut microbes themselves instead of the human host in which they reside.

EXPERIMENTAL PROCEDURES

Human Studies

To examine whether circulating choline and TMAO levels were associated with T2DM risk, we recruited two unique cohorts including both men and women

with diverse cardiometabolic risk profiles in cardiology and hepatology clinics at the Cleveland Clinic. These studies were approved by the Cleveland Clinic Institutional Review Board, and every subject provided written informed consent. Extended patient demographics, laboratory values, and clinical characteristics are available in [Supplemental Experimental Procedures](#). To examine the relationship between *FMO3* expression and metabolic traits, we took advantage of adipose biopsy microarray data ($n = 770$) within the Metabolic Syndrome in Men (METSIM) study, which has been previously described in detail ([Stancáková et al., 2009](#)). The study was approved by the ethics committee of the University of Eastern Finland and Kuopio University Hospital and was conducted in accordance with the Helsinki Declaration. All study participants gave written informed consent. To validate human adipose microarray findings from the METSIM cohort, we analyzed additional microarray data from two distinct cohorts spanning both men and women of European American and African American ethnicity, which have previously been described ([Das et al., 2015](#); [Sharma et al., 2016](#)). These studies were approved by the University of Arkansas for Medical Sciences and the Institutional Review Board of Wake Forest School of Medicine. All study participants gave written informed consent. Finally, we examined the protein expression of *FMO3* in human liver from normal BMI or bariatric surgery patients. This study was approved by the Institutional Review Board of Wake Forest School of Medicine, and all study participants gave written informed consent. Detailed information for all human studies is provided in [Supplemental Experimental Procedures](#).

Animal Studies

To study the role of the TMAO-producing enzyme *FMO3* in diet-induced obesity, we initially employed an *in vivo* ASO-mediated knockdown approach as previously described ([Warrier et al., 2015](#); [Shih et al., 2015](#)). Because of the known sexual dimorphism of hepatic *FMO3* expression in mice, all studies were conducted in adult female mice unless otherwise noted. Mice were maintained on either standard rodent chow (2918 Teklad Global 18% Protein Rodent Diet) or a custom high-fat diet composed of 45% kcal derived from fat ([Brown et al., 2010](#)). ASO-treated mice were then subjected to cold tolerance and indirect calorimetry studies using methods previously described ([Thomas et al., 2013](#)). To establish *FMO3* knockout mice, we used CRISPR-Cas9 gene editing as described in [Supplemental Experimental Procedures](#). Plasma TMA and TMAO quantification and *FMO* activity measurements were measured using stable isotope dilution mass spectrometry-based assays as previously described ([Wang et al., 2014](#); [Warrier et al., 2015](#)) on a Shimadzu 8050 triple quadrupole mass spectrometer. All mouse studies were approved by Institutional Animal Care and Use Committees of the Cleveland Clinic, Case Western Reserve University, or University of California, Los Angeles. Detailed information for all mouse studies and biochemical workup of mouse tissue is provided in [Supplemental Experimental Procedures](#).

Statistical Analysis

To examine the association between circulating choline and TMAO with T2DM, Wilcoxon rank-sum tests were used for continuous variables, and χ^2 tests were used for categorical variables. Multilogistic regression models were used to estimate odds ratio and 95% confidence interval for diabetes. All analyses were performed using R 3.1.0, and $p \leq 0.05$ was considered statistically significant. All mouse data were analyzed using either one-way or two-way ANOVA, where appropriate, followed by post hoc analysis. Differences were considered significant at $p \leq 0.05$. All mouse data analyses were performed using JMP Pro 10 (SAS Institute) or GraphPad Prism 6 software.

SUPPLEMENTAL INFORMATION

Supplemental Information includes Supplemental Experimental Procedures, four figures, and five tables and can be found with this article online at <http://dx.doi.org/10.1016/j.celrep.2017.05.077>.

AUTHOR CONTRIBUTIONS

R.C.S., D.M.S., M.W., and J.M.B. planned the project, designed experiments, analyzed data, and wrote the manuscript; J.M.B., S.L.H., S.V.N.P., W.H.W.T.,

A.J.L., M.C., and M.L. designed experiments and provided useful discussion directing the project; R.C.S., D.M.S., M.W., R.N.H., A.B., D.F., A.L.B., A.D.G., M.H., A.C., L.L., X.S.L., Z.W., B.W., Y.M., H.K., N.C., C.P., R.E.M., C.D.L., S.K.D., L.L.R., N.Z., A.J.M., S.D., M.L., M.C., and J.H. either recruited human subjects or conducted mouse experiments, performed biochemical workup of mouse tissues, analyzed data, and aided in manuscript preparation; B.O.E and C.A.F. performed imaging studies in mice; R.G.L., R.M.C., and M.J.G. provided antisense oligonucleotides; and all authors were involved in the editing of the final manuscript.

ACKNOWLEDGMENTS

This work was supported by NIH and Office of Dietary Supplements grants R00 HL096166 (J.M.B.), R01 HL122283 (J.M.B.), P50 AA024333 (J.M.B.), R01 HL103866 (S.L.H.), R01 HL126827 (S.L.H. and W.H.W.T.), R01 DK106000 (S.L.H. and W.H.W.T.), R01 HL130819 (Z.W.), R01 DK090111 (S.K.D.), R00 HL12172 (M.C.), P01 HL028481 (A.J.L.), P01 HL030568-31A1 (A.J.L. and D.M.S.), and P01 HL49373 (L.L.R.), as well as by the Deutsche Forschungsgemeinschaft in the framework of SFB841 (J.H.), the Academy of Finland and the Finnish Cardiovascular Research Foundation (M.L.), and the American Heart Association (postdoctoral fellowship 15POST2535000 to R.C.S., postdoctoral fellowship 14POST18700001 to M.W., and postdoctoral fellowship 17POST3285000 to R.N.H.).

S.L.H. and Z.W. are named as co-inventors on pending and issued patents held by the Cleveland Clinic relating to cardiovascular diagnostics and therapeutics. S.L.H. reports he has been paid as a consultant by Esperion and Procter & Gamble. S.L.H. has received research funds from Astra Zeneca, Procter & Gamble, Roche, and Takeda. S.L.H. has the rights to receive royalty payments for inventions or discoveries related to cardiovascular diagnostics from Cleveland Heart Lab Inc., Frantz Biomarkers, and Siemens Healthcare. R.G.L., R.M.C., and M.J.G. are employees of Ionis Pharmaceuticals, Inc. (Carlsbad, CA).

Received: April 13, 2016

Revised: May 2, 2017

Accepted: May 23, 2017

Published: June 20, 2017

REFERENCES

- Bäckhed, F., Ding, H., Wang, T., Hooper, L.V., Koh, G.Y., Nagy, A., Semenkovich, C.F., and Gordon, J.I. (2004). The gut microbiota as an environmental factor that regulates fat storage. *Proc. Natl. Acad. Sci. USA* *101*, 15718–15723.
- Bartelt, A., and Heeren, J. (2014). Adipose tissue browning and metabolic health. *Nat. Rev. Endocrinol.* *10*, 24–36.
- Bennett, B.J., de Aguiar Vallim, T.Q., Wang, Z., Shih, D.M., Meng, Y., Gregory, J., Allayee, H., Lee, R., Graham, M., Crooke, R., et al. (2013). Trimethylamine-N-oxide, a metabolite associated with atherosclerosis, exhibits complex genetic and dietary regulation. *Cell Metab.* *17*, 49–60.
- Brown, J.M., Betters, J.L., Lord, C., Ma, Y., Han, X., Yang, K., Alger, H.M., Melchior, J., Sawyer, J., Shah, R., et al. (2010). CGI-58 knockdown in mice causes hepatic steatosis but prevents diet-induced obesity and glucose intolerance. *J Lipid Res.* *51*, 3306–3315.
- Brown, J.M., and Hazen, S.L. (2015). The gut microbial endocrine organ: bacterially derived signals driving cardiometabolic diseases. *Annu. Rev. Med.* *66*, 343–359.
- Cashman, J.R., and Zhang, J. (2006). Human flavin-containing monooxygenases. *Annu. Rev. Pharmacol. Toxicol.* *46*, 65–100.
- Civelek, M., Wu, Y., Pan, C., Raulerson, C.K., Ko, A., He, A., Tilford, C., Saleem, N.K., Stancáková, A., Scott, L.J., et al. (2017). Genetic regulation of adipose gene expression and cardio-metabolic traits. *Am. J. Hum. Genet.* *100*, 428–443.
- Cox, L.M., Yamanishi, S., Sohn, J., Alekseyenko, A.V., Leung, J.M., Cho, I., Kim, S.G., Li, H., Gao, Z., Mahana, D., et al. (2014). Altering the intestinal

- microbiota during a critical developmental window has lasting metabolic consequences. *Cell* 158, 705–721.
- Dambrova, M., Latkovskis, G., Kuka, J., Strele, I., Konrade, I., Grinberga, S., Hartmane, D., Pugovics, O., Erglis, A., and Liepinsh, E. (2016). Diabetes is associated with higher trimethylamine N-oxide plasma levels. *Exp. Clin. Endocrinol. Diabetes* 124, 251–256.
- Das, S.K., Sharma, N.K., and Zhang, B. (2015). Integrative network analysis reveals different pathophysiological mechanisms of insulin resistance among Caucasians and African Americans. *BMC Med. Genomics* 8, 4.
- Gao, X., Liu, X., Xu, J., Xue, C., Xue, Y., and Wang, Y. (2014). Dietary trimethylamine N-oxide exacerbates impaired glucose tolerance in mice fed a high fat diet. *J. Biosci. Bioeng.* 118, 476–481.
- Gregory, J.C., Buffa, J.A., Org, E., Wang, Z., Levison, B.S., Zhu, W., Wagner, M.A., Bennett, B.J., Li, L., DiDonato, J.A., et al. (2015). Transmission of atherosclerosis susceptibility with gut microbial transplantation. *J. Biol. Chem.* 290, 5647–5660.
- Jiang, X., Yan, J., West, A.A., Perry, C.A., Malysheva, O.V., Devapatla, S., Pressman, E., Vermeylen, F., and Caudill, M.A. (2012). Maternal choline intake alters the epigenetic state of fetal cortisol-regulating genes in humans. *FASEB J.* 26, 3563–3574.
- Koeth, R.A., Wang, Z., Levison, B.S., Buffa, J.A., Org, E., Sheehy, B.T., Britt, E.B., Fu, X., Wu, Y., Li, L., et al. (2013). Intestinal microbiota metabolism of L-carnitine, a nutrient in red meat, promotes atherosclerosis. *Nat. Med.* 19, 576–585.
- Koeth, R.A., Levison, B.S., Culley, M.K., Buffa, J.A., Wang, Z., Gregory, J.C., Org, E., Wu, Y., Li, L., Smith, J.D., et al. (2014). γ -Butyrobetaine is a proatherogenic intermediate in gut microbial metabolism of L-carnitine to TMAO. *Cell Metab.* 20, 799–812.
- Lever, M., George, P.M., Slow, S., Bellamy, D., Young, J.M., Ho, M., McEntyre, C.J., Elmslie, J.L., Atkinson, W., Molyneux, S.L., et al. (2014). Betaine and trimethylamine-N-oxide as predictors of cardiovascular outcomes show different patterns in diabetes mellitus: an observational study. *PLoS ONE* 9, e114969.
- Ley, R.E., Bäckhed, F., Turnbaugh, P., Lozupone, C.A., Knight, R.D., and Gordon, J.I. (2005). Obesity alters gut microbial ecology. *Proc. Natl. Acad. Sci. USA* 102, 11070–11075.
- Li, Q., Korzan, W.J., Ferrero, D.M., Chang, R.B., Roy, D.S., Buchi, M., Lemon, J.K., Kaur, A.W., Stowers, L., Fendt, M., and Liberles, S.D. (2013). Synchronous evolution of an odor biosynthesis pathway and behavioral response. *Curr. Biol.* 23, 11–20.
- Mafune, A., Iwamoto, T., Tsutsumi, Y., Nakashima, A., Yamamoto, I., Yokoyama, K., Yokoo, T., and Urashima, M. (2016). Associations among serum trimethylamine-N-oxide (TMAO) levels, kidney function and infarcted coronary artery number in patients undergoing cardiovascular surgery: a cross-sectional study. *Clin. Exp. Nephrol.* 20, 731–739.
- Matsuda, M., and DeFronzo, R.A. (1999). Insulin sensitivity indices obtained from oral glucose tolerance testing: comparison with the euglycemic insulin clamp. *Diabetes Care* 22, 1462–1470.
- Miao, J., Ling, A.V., Manthena, P.V., Gearing, M.E., Graham, M.J., Crooke, R.M., Croce, K.J., Esquejo, R.M., Clish, C.B., Vicent, D., and Biddinger, S.B.; Morbid Obesity Study Group (2015). Flavin-containing monooxygenase 3 as a potential player in diabetes-associated atherosclerosis. *Nat. Commun.* 6, 6498.
- Missailidis, C., Hällqvist, J., Qureshi, A.R., Barany, P., Heimbürger, O., Lindholm, B., Stenvinkel, P., and Bergman, P. (2016). Serum trimethylamine-N-oxide is strongly related to renal function and predicts outcome in chronic kidney disease. *PLoS ONE* 11, e0141738.
- Muoio, D.M. (2014). Metabolic inflexibility: when mitochondrial indecision leads to metabolic gridlock. *Cell* 159, 1253–1262.
- Parks, B.W., Nam, E., Org, E., Kostem, E., Norheim, F., Hui, S.T., Pan, C., Civelek, M., Rau, C.D., Bennett, B.J., et al. (2013). Genetic control of obesity and gut microbiota composition in response to high-fat, high-sucrose diet in mice. *Cell Metab.* 17, 141–152.
- Poly, C., Massaro, J.M., Seshadri, S., Wolf, P.A., Cho, E., Krall, E., Jacques, P.F., and Au, R. (2011). The relation of dietary choline to cognitive performance and white-matter hyperintensity in the Framingham Offspring Cohort. *Am. J. Clin. Nutr.* 94, 1584–1591.
- Puigserver, P., Wu, Z., Park, C.W., Graves, R., Wright, M., and Spiegelman, B.M. (1998). A cold-inducible coactivator of nuclear receptors linked to adaptive thermogenesis. *Cell* 92, 829–839.
- Romano, K.A., Vivas, E.I., Amador-Noguez, D., and Rey, F.E. (2015). Intestinal microbiota composition modulates choline bioavailability from diet and accumulation of the proatherogenic metabolite trimethylamine-N-oxide. *MBio* 6, e02481.
- Sharma, N.K., Sajuthi, S.P., Chou, J.W., Calles-Escandon, J., Demons, J., Rogers, S., Ma, L., Palmer, N.D., McWilliams, D.R., Beal, J., et al. (2016). Tissue-specific and genetic regulation of insulin sensitivity-associated transcripts in African Americans. *J. Clin. Endocrinol. Metab.* 101, 1455–1468.
- Shaw, G.M., Finnell, R.H., Blom, H.J., Carmichael, S.L., Vollset, S.E., Yang, W., and Ueland, P.M. (2009). Choline and risk of neural tube defects in a folate-fortified population. *Epidemiology* 20, 714–719.
- Shih, D.M., Wang, Z., Lee, R., Meng, Y., Che, N., Charugundla, S., Qi, H., Wu, J., Pan, C., Brown, J.M., et al. (2015). Flavin containing monooxygenase 3 exerts broad effects on glucose and lipid metabolism and atherosclerosis. *J. Lipid Res.* 56, 22–37.
- Stancáková, A., Kuulasmaa, T., Paananen, J., Jackson, A.U., Bonnycastle, L.L., Collins, F.S., Boehnke, M., Kuusisto, J., and Laakso, M. (2009). Association of 18 confirmed susceptibility loci for type 2 diabetes with indices of insulin release, proinsulin conversion, and insulin sensitivity in 5,327 nondiabetic Finnish men. *Diabetes* 58, 2129–2136.
- Suzuki, T., Heaney, L.M., Bhandari, S.S., Jones, D.J., and Ng, L.L. (2016). Trimethylamine N-oxide and prognosis in acute heart failure. *Heart* 102, 841–848.
- Tang, W.H., Wang, Z., Levison, B.S., Koeth, R.A., Britt, E.B., Fu, X., Wu, Y., and Hazen, S.L. (2013). Intestinal microbial metabolism of phosphatidylcholine and cardiovascular risk. *N. Engl. J. Med.* 368, 1575–1584.
- Tang, W.H., Wang, Z., Fan, Y., Levison, B., Hazen, J.E., Donahue, L.M., Wu, Y., and Hazen, S.L. (2014). Prognostic value of elevated levels of intestinal microbe-generated metabolite trimethylamine-N-oxide in patients with heart failure: refining the gut hypothesis. *J. Am. Coll. Cardiol.* 64, 1908–1914.
- Tang, W.H., Wang, Z., Li, X.S., Fan, Y., Li, D.S., Wu, Y., and Hazen, S.L. (2017). Increased trimethylamine N-oxide portends high mortality risk independent of glycemic control in patients with type 2 diabetes mellitus. *Clin. Chem.* 63, 297–306.
- Thomas, G., Betters, J.L., Lord, C.C., Brown, A.L., Marshall, S., Ferguson, D., Sawyer, J., Davis, M.A., Melchior, J.T., Blume, L.C., et al. (2013). The serine hydrolase ABHD6 is a critical regulator of the metabolic syndrome. *Cell Rep.* 5, 508–520.
- Trosetid, M., Ueland, T., Hov, J.R., Svardsdal, A., Gregersen, I., Dahl, C.P., Aakhus, S., Gude, E., Bjørndal, B., Halvorsen, B., et al. (2015). Microbiota-dependent metabolite trimethylamine-N-oxide is associated with disease severity and survival of patients with chronic heart failure. *J. Intern. Med.* 277, 717–726.
- Turnbaugh, P.J., and Gordon, J.I. (2009). The core gut microbiome, energy balance and obesity. *J. Physiol.* 587, 4153–4158.
- Ussar, S., Lee, K.Y., Dankel, S.N., Boucher, J., Haering, M.F., Kleinridders, A., Thomou, T., Xue, R., Macotela, Y., Cypess, A.M., et al. (2014). ASC-1, PAT2, and P2RX5 are cell surface markers for white, beige, and brown adipocytes. *Sci. Transl. Med.* 6, 247ra103.
- Wang, Z., Klipfelf, E., Bennett, B.J., Koeth, R., Levison, B.S., Dugar, B., Feldstein, A.E., Britt, E.B., Fu, X., Chung, Y.M., et al. (2011). Gut flora metabolism of phosphatidylcholine promotes cardiovascular disease. *Nature* 472, 57–63.
- Wang, Z., Tang, W.H., Buffa, J.A., Fu, X., Britt, E.B., Koeth, R.A., Levison, B.S., Fan, Y., Wu, Y., and Hazen, S.L. (2014). Prognostic value of choline and betaine depends on intestinal microbiota-generated metabolite trimethylamine-N-oxide. *Eur. Heart J.* 35, 904–910.
- Wang, Z., Roberts, A.B., Buffa, J.A., Levison, B.S., Zhu, W., Org, E., Gu, X., Huang, Y., Zamanian-Daryoush, M., Culley, M.K., et al. (2015). Non-lethal

inhibition of gut microbial trimethylamine production for the treatment of atherosclerosis. *Cell* 163, 1585–1595.

Warrier, M., Shih, D.M., Burrows, A.C., Ferguson, D., Gromovsky, A.D., Brown, A.L., Marshall, S., McDaniel, A., Schugar, R.C., Wang, Z., et al. (2015). The TMAO-generating enzyme flavin monooxygenase 3 is a central regulator of cholesterol balance. *Cell Rep.* 10, 1–13.

Wu, J., Boström, P., Sparks, L.M., Ye, L., Choi, J.H., Giang, A.H., Khandekar, M., Virtanen, K.A., Nuutila, P., Schaart, G., et al. (2012). Beige adipocytes are a distinct type of thermogenic fat cell in mouse and human. *Cell* 150, 366–376.

Zhu, W., Gregory, J.C., Org, E., Buffa, J.A., Gupta, N., Wang, Z., Li, L., Fu, X., Wu, Y., Mehrabian, M., et al. (2016). Gut microbial metabolite TMAO enhances platelet hyperreactivity and thrombosis risk. *Cell* 165, 111–124.

Supplemental Information

The TMAO-Producing Enzyme Flavin-Containing Monooxygenase 3 Regulates Obesity and the Beiging of White Adipose Tissue

Rebecca C. Schugar, Diana M. Shih, Manya Warriar, Robert N. Helsley, Amy Burrows, Daniel Ferguson, Amanda L. Brown, Anthony D. Gromovsky, Markus Heine, Arunachal Chatterjee, Lin Li, Xinmin S. Li, Zeneng Wang, Belinda Willard, YongHong Meng, Hanjun Kim, Nam Che, Calvin Pan, Richard G. Lee, Rosanne M. Crooke, Mark J. Graham, Richard E. Morton, Carl D. Langefeld, Swapan K. Das, Lawrence L. Rudel, Nizar Zein, Arthur J. McCullough, Srinivasan Dasarathy, W.H. Wilson Tang, Bernadette O. Erokwu, Chris A. Flask, Markku Laakso, Mete Civelek, Sathyamangla V. Naga Prasad, Joerg Heeren, Aldons J. Lusic, Stanley L. Hazen, and J. Mark Brown

Supplemental Table 1. Characteristics of Preventive Cardiology Cohort, Related to Figure 1

Factor	Total (N=187)	No Diabetes (N=145)	Diabetes (N=42)	p-value*
Demographic				
Age	51.1±12.0	49.7 ±11.8	55.9±11.6	0.0034
Male (%)	98 (52.4)	77 (53.1)	21 (50.0)	0.8578
Current Smoker (%)	45 (24.1)	40 (27.6)	5 (11.9)	0.0590
BMI	29.4(26.4-35.1)	28.7(25.8-33.9)	32.8(28.4-38.1)	0.00013
Clinical				
BPS	126.0(117.2-137.0)	123.5(114.8-136.2)	130.0(122.0-141.8)	0.0323
BPD	77.0(70.0-84.0)	77.0(70.0-83.3)	79(71.0-88.8)	0.2880
Cholesterol	180.0(157.5-208.0)	179.0(158.0-205.0)	187.5(147.5-223.2)	0.4258
Triglycerides	122.0(87.0-178.0)	118.0(87.0-166.0)	135.5(98.3-217.8)	0.0624
HDL	43.0(35.5-51.5)	44.0(36.0-54.0)	41.0(35.5-47.8)	0.2962
LDL	107.0(88.0-131.0)	106.0(89.0-129.0)	107.5(78.8-146.5)	0.9445
CRP	1.8(0.5-5.5)	1.6(0.5-4.9)	2.3(0.9-7.6)	0.1874
HgbA1c	5.2(4.9-6.0)	5.1(4.7-5.5)	6.25(5.9-7.7)	<0.0001
Glucose/Insulin	7.8(5.1-14.7)	9.44(5.7-17.1)	5.78(3.5-9.6)	0.6402
TMAO	3.4(2.1-5.4)	3.1(2.1-4.9)	4.7(3.1-7.0)	0.00086
Choline	8.0(6.6-9.8)	7.9(6.6-9.7)	8.3(6.6-10.0)	0.5798
Betaine	41.1(30.6-51.6)	44.6(33.5-53.2)	31.8(26.8-41.8)	<0.0001

*p values were calculated by Wilcoxon-test for continuous data and Pearson's chi-square test for categorical factors.

Supplemental Table 2. Characteristics of Hepatology Cohort, Related to Figure 1

Factor	Total (N=248)	No Diabetes (N=188)	Diabetes (N=60)	p-value*
Demographic				
Age	60.7±13.1	60.3 ±14.3	62.2±7.9	0.7676
Male (%)	132 (53.2)	98 (52.1)	34 (56.7)	0.6420
Current Smoker (%)	17 (6.9)	10 (5.3)	7 (11.7)	0.1613
BMI	29.2(25.5-32.3)	28.0(25.1-31.4)	31.2(28.4-34.9)	0.00015
Clinical				
BPS	122.0(112.0-130.0)	120.0(112.0-130.0)	122.0(114.8-130.0)	0.5184
BPD	72.0(68.0-80.0)	74.0(68.0-80.0)	70(64.0-78.0)	0.0024
Cholesterol	165.0(137.0-205.0)	169.0(139.0-212.0)	155.5(131.5-180.5)	0.0298
Triglycerides	99.0(71.0-142.5)	93.0(69.5-135.0)	125.5(79.8-188.8)	0.00075
HDL	47.0(39.0-55.0)	49.0(41.0-57.5)	41.5(34.8-47.3)	<0.0001
LDL	96.0(70.5-122.5)	99.0(75.0-127.0)	84.5(64.3-103.5)	0.0084
CRP	1.4(0.6-3.45)	1.3(0.5-2.70)	2.2(1.15-7.4)	0.00018
HgbA1c	5.4(5.1-5.8)	5.3(5.0-5.6)	6.3(5.6-6.9)	<0.0001
Glucose/Insulin	11.4(7.7-16.2)	12.5(8.9-18.3)	7.2(4.0-11.4)	0.0022
TMAO	3.6(2.4-5.2)	3.3(2.3-5.2)	5.0(3.3-9.3)	<0.0001
Choline	6.9(5.7-8.4)	6.7(5.6-8.1)	8.0(6.3-9.5)	0.00046
Betaine	38.3(29.0-49.8)	38.9(29.7-49.5)	35.6(27.4-51.7)	0.3580

*p values were calculated by Wilcoxon-test for continuous data and Pearson's chi-square test for categorical factors.

Supplemental Table 3. Characteristics of Combined Cardiology and Hepatology Cohorts, Related to Figure 1

Factor	Total (N=435)	No Diabetes (N=333)	Diabetes (N=102)	p-value*
Demographic				
Age	56.6±13.5	55.6 ±14.3	59.6±10.0	0.0142
Male (%)	230 (52.9)	175 (52.6)	55 (53.9)	0.8974
Current Smoker (%)	62 (14.3)	50 (15.0)	12 (11.8)	0.5094
BMI	29.3(25.8-33.2)	28.4(25.4-32.4)	31.6(28.4-36.3)	<0.0001
Clinical				
BPS	122.0(114.0-133.0)	122.0(113.0-132.0)	126.0(117.2-134.5)	0.0633
BPD	74.0(68.0-81.0)	75.0(69.0-80.3)	74(66.0-81.8)	0.3627
Cholesterol	173.0(146.0-207.0)	177.0(148.0-208.0)	166.0(138.2-205.8)	0.1089
Triglycerides	107.5(78.0-155.8)	103.0(76.0-148.2)	127.5(84.0-203.2)	0.00025
HDL	45.5(37.0-55.0)	46.0(38.0-56.0)	41.0(35.0-47.8)	0.00015
LDL	101.0(77.0-126.8)	104.0(80.0-129.0)	96.5(72.0-120.0)	0.0246
CRP	1.6(0.6-4.4)	1.4(0.5-3.8)	2.3(1.0-7.4)	0.00035
HgbA1c	5.3(5.0-5.9)	5.2(4.9-5.5)	6.3(5.7-7.1)	<0.0001
Glucose/Insulin	9.8(6.5-15.4)	10.8(6.6-17.5)	6.6(3.8-11.2)	0.0127
TMAO	3.5(2.4-5.6)	3.2(2.2-5.1)	4.8(3.3-7.7)	<0.0001
Choline	7.5(6.1-9.1)	7.3(6.0-8.7)	8.1(6.4-9.6)	0.0025
Betaine	39.3(29.9-51.1)	41.0(30.3-51.7)	33.8(27.2-45.1)	0.00063

*p values were calculated by Wilcoxon-test for continuous data and Pearson's chi-square test for categorical factors.

Supplemental Table 4. Dietary levels of free and lipid choline quantified by Liquid Chromotography-Tandem Mass Spectrometry, Related to Figure 3

	Free Choline (mg/100mg diet)	Lipid Choline (mg/100 mg diet)	Total Choline (mg/100 mg/diet)
Chow	9.69	2.65	12.34
High Fat Diet	8.79	0.26	9.05

Supplemental Table 5. *Fmo3* mutations identified in *Fmo3* mutant mice generated by the CRISPR/Cas9 technology, Related to Figure 5

Identified <i>Fmo3</i> mutation*	Predicted mutation in FMO3 protein
1 bp insertion (A) at bp 89 of exon 2	Frameshift, premature termination at a.a.-pos 74
7 bps deletion (bps 87-93) of exon 2	Frameshift, premature termination at a.a.-pos 98
6 bps deletion (bps 88-93) of exon 2	Two a.a. in-frame deletion (74-75 a.a.-pos)
1 bp insertion (T) at bp 90 of exon 2	Frameshift, premature termination at a.a.-pos 76
1 bp deletion (T) at bp 90 of exon 2	Frameshift, premature termination at a.a.-pos 100

*: All mutations are located in the exon 2 of *Fmo3* gene, bp: base pair

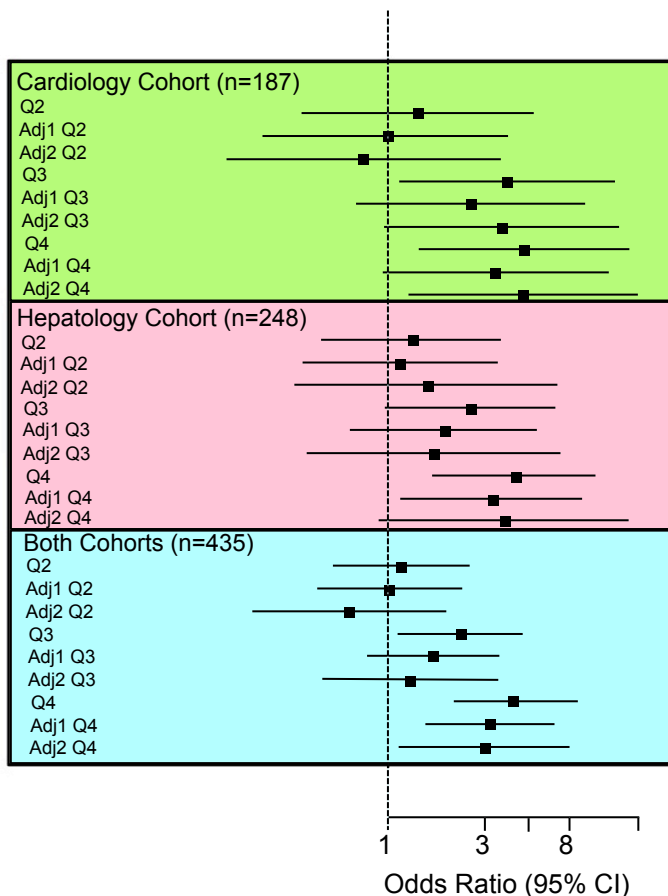
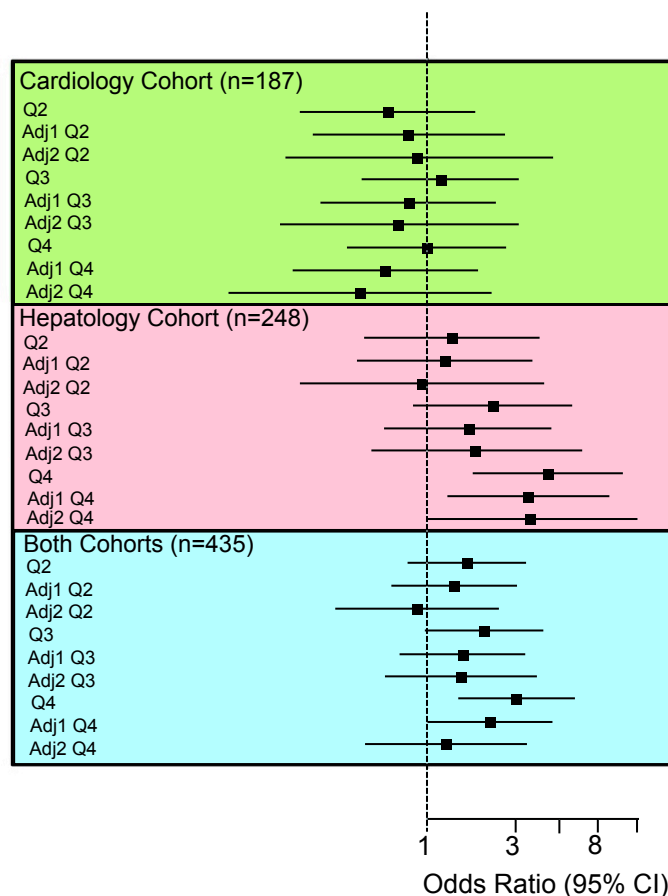
A**TMAO Quartiles****B****Choline Quartiles**

Figure S1. After Adjustments for Multiple Comorbidities, Prevalent CVD and CVD Risk Factors, Medications, and Renal Function, TMAO Remains a Strong Predictor of T2DM Risk, Related to Figure 1.

We recruited two separate cohorts of stable subjects in preventative cardiology (n=187) or hepatology clinics (n=248) to evaluate associations between fasting circulating TMAO or choline levels with prevalent type 2 diabetes (T2DM). The total number of subjects recruited in both studies was n=435. Patient demographics, laboratory values, and clinical characteristics are provided in detail in the Supplemental Table 1.

(A) Forest plots of the odds ratio of prevalent T2DM and quartiles of TMAO; bars represent 95% confidence intervals.

(B) Forest plots of the odds ratio of prevalent T2DM and quartiles of choline; bars represent 95% confidence intervals.

Adjusted Model 1 = Adj1: Adjusted for age, gender, current smoker, BMI, and systolic blood pressure.

Adjusted Model 2 = Adj2: Adjusted for age, gender, current smoker, BMI, and systolic blood pressure, glucose, triglycerides, HDL, and medication class.

Medication Classes Included: Analgesic-Aspirin, Analgesic-NSAID, Analgesic-Other, Cardiology-Antiarrhythmic, Cardiology-Anticoagulant, Cardiology-Other, Diabetes-Combo, Diabetes-Insulin, Diabetes-Other, Diabetes-Sulfonylurea, Diuretic-Fluid, Diuretic-Other, Food Suppl., GI-Antihistamine, GI-Other, HTN-A2 Receptors, HTN-Ace, HTN-Alpha 1, HTN-Beta Blocker, HTN-CCB, HTN-Central, HTN-Combination, HTN-Diuretic, HTN-Other, HTN-Peripheral, Infectious Antibiotic, Lipid Lower-Fibric Acid, Lipid Lower-Fish Oil, Lipid Lower-Niacin, Lipid Lower-Resin, Lipid Lower-Statin, Lipid Lower-Other, Mineral Suppl.-Other, Mineral Suppl.-Calcium, Mineral Suppl.-Iron, Nitrate, Psyche-Antidepressant, Psyche-Antianxiety, Psyche-Nontraditional, Psyche-Other, Respiratory-Steroid, Respiratory-Other, Steroid Hormones, and Vitamins.

A**Validation Cohort #1: European American (n=99)**

	Body Mass Index		Fat %		Insulin Sensitivity		WAT <i>UCP1</i> Expression	
	<i>r</i>	<i>p</i>	<i>r</i>	<i>p</i>	<i>r</i>	<i>p</i>	<i>r</i>	<i>p</i>
<i>FMO3</i> - v1	0.23	2.40E-02	0.23	2.30E-02	-0.35	4.0E-04	-0.22	3.17E-02
<i>FMO3</i> - v2	0.17	8.60E-02	0.17	1.00E-01	-0.32	1.0E-03	No Data	No Data

B**Validation Cohort #2: African American (n=256)**

	Body Mass Index		Matsuda Index		Insulin Sensitivity		WAT <i>PRDM16</i> Expression	
	<i>r</i>	<i>p</i>	<i>r</i>	<i>p</i>	<i>r</i>	<i>p</i>	<i>r</i>	<i>p</i>
<i>FMO3</i> - v1	0.23	2.91E-04	-0.16	1.0E-02	-0.15	2.1E-02	-0.27	1.6E-05
<i>FMO3</i> - v2	0.30	1.66E-06	-0.20	2.0E-03	-0.18	7.0E-03	No Data	No Data

Figure S2. Validation Cohorts for Examining the Association Between Human White Adipose Tissue (WAT) *FMO3* Expression and Metabolic Traits, Related to Figure 2.

To confirm findings in the large METSIM study, which only includes Finnish men, we examined the relationship between WAT *FMO3* expression and metabolic traits in two additional cohorts spanning both men and women of European American and African American ethnicity. The first cohort (panel A) included n=99 non-Hispanic Caucasian Americans, including 42 males and 57 females (Das et al., 2015). The second cohort (panel B) included n=260 African Americans, including 139 males and 121 females (Sharma et al., 2016). Data show the correlation between the two major *FMO3* transcript variants (v1, NM_001002294.1; v2, NM_006894.4) and metabolic traits. In addition, the correlation between WAT *FMO3* and markers of brown/beige adipocytes (*PRDM16* and *UCP1*) is shown.

(A) Correlation between human WAT *FMO3* mRNA expression and metabolic traits in European American men and women (n=99).

(B) Correlation between human WAT *FMO3* mRNA expression and metabolic traits in African American men and women (n=260).

Abbreviations: *PRDM16*, PR domain containing 16, *UCP1*, uncoupling protein 1.

A Human Liver Biopsy Cohort Subject Characteristics

	BMI <30 (n=10)	BMI ≥30 (n=40)	p value
Age	50.90 ±4.30	46.35 ±2.00	0.3217
Female (%)	60.0	72.5	-
Weight (lbs)	157.74 ±8.03	235.99 ±17.00	0.0278
Insulin (μIU/ml)	6.78 ±2.75	9.41 ±1.58	0.4925
Fasting Glucose (mg/dl)	95.34 ±9.83	121.57 ±6.05	0.0508
HOMA-IR	2.03 ±1.03	3.36 ±0.84	0.4451
Plasma Cholesterol (mg/dl)	122.35 ±32.44	131.32 ±9.05	0.7112
Plasma Triglycerides (mg/dl)	172.84 ±10.37	169.90 ±7.23	0.8496
Liver Triglycerides (mg/g PR)	284.37 ±150.93	407.04 ±64.96	0.4174

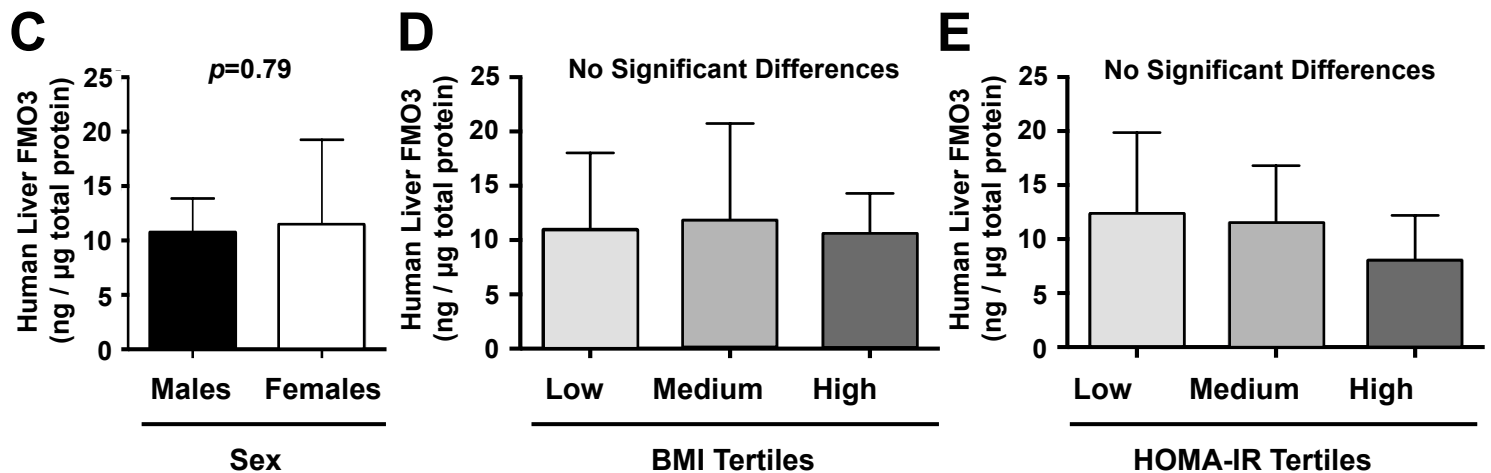
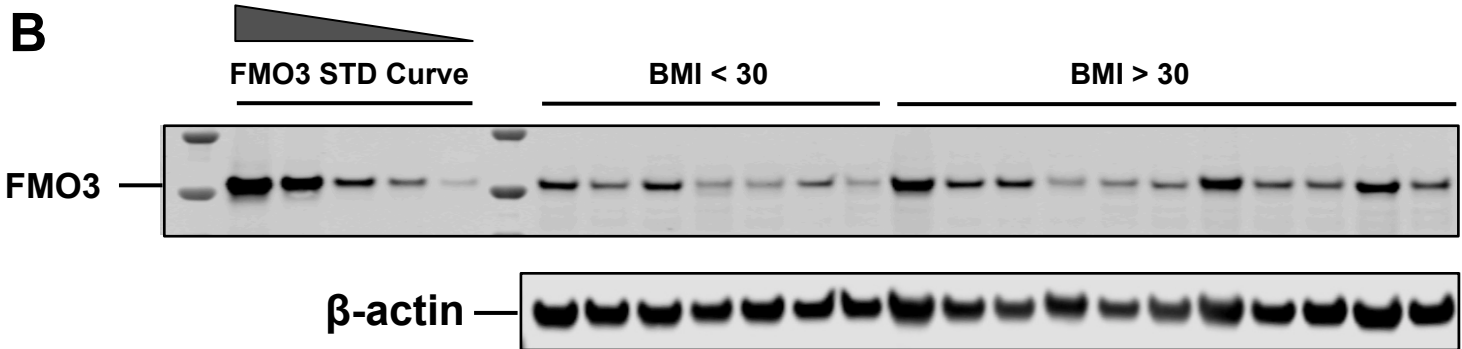


Figure S3. FMO3 Protein Expression in Human Liver, Related to Figure 2.

We recruited a cohort of surgical patients with a wide range of body mass index (BMI), and performed quantitative Western blotting to determine the abundance of FMO3 protein expression in relation to BMI. The total number of human livers assayed for FMO3 protein abundance was n=50.

(A) Patient demographics, laboratory values, and clinical characteristics separated by BMI.

(B) Representative Western blot showing a single band corresponding to the molecular weight of a recombinant hFMO3 protein standard curve.

(C) FMO3 protein abundance is not sexually dimorphic in human liver.

(D) FMO3 protein abundance is not different between low, medium, and high tertiles of BMI.

(E) FMO3 protein abundance is not different between low, medium, and high tertiles of Homeostatic Model Assessment of Insulin Resistance (HOMA-IR).

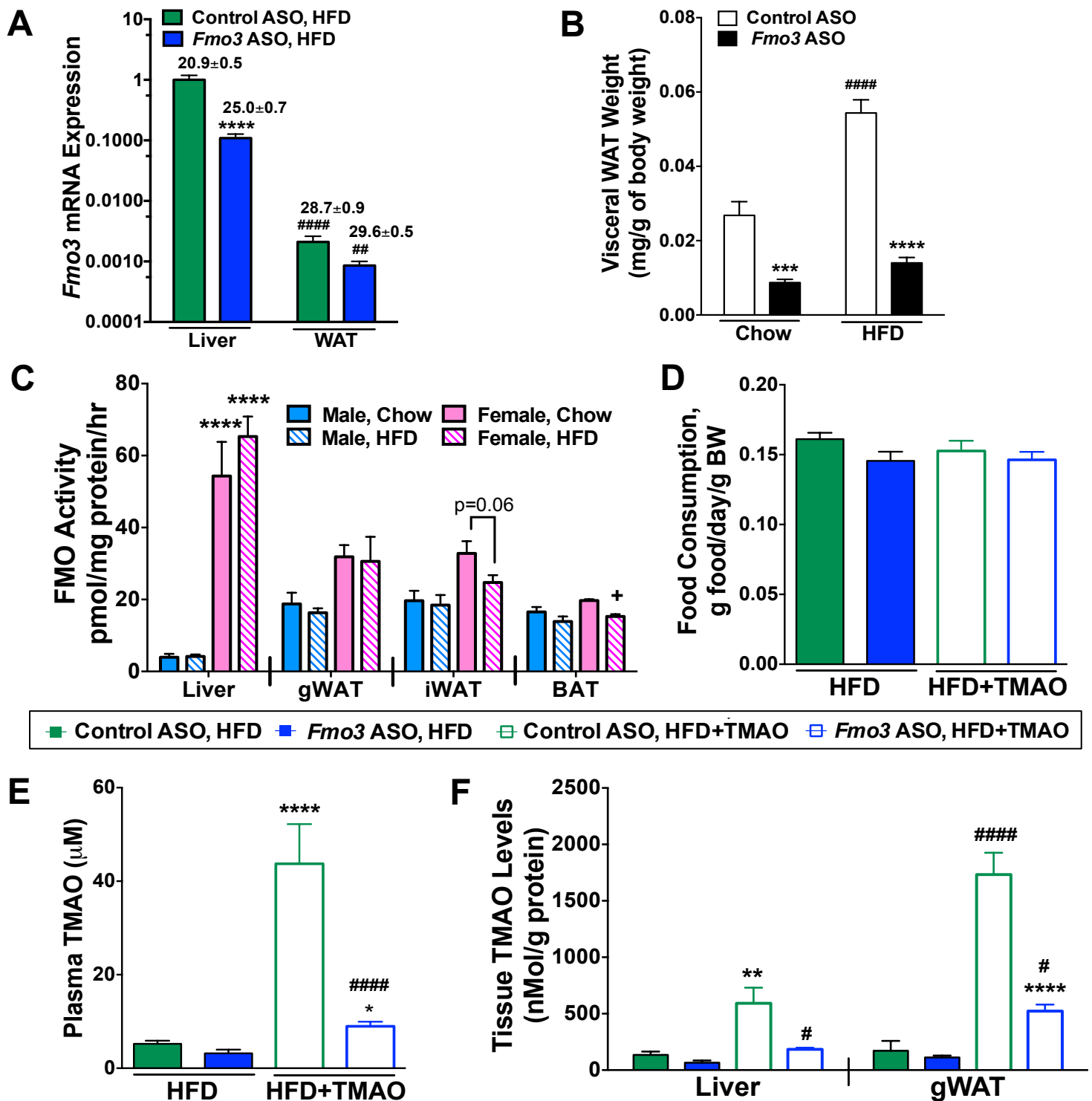


Figure S4. Alterations in the TMA/FMO3/TMAO Pathway in Mouse Studies, Related to Figure 4.

At 6-8 weeks of age, male and female C57BL/6 mice were treated with either a non-targeting control ASO or an ASO targeting knockdown of FMO3 in conjunction with either standard rodent chow or high fat diet (HFD) feeding as indicated.

(A) Relative *Fmo3* gene expression in matched liver and gonadal white adipose tissue samples of female mice fed HFD. Numerical values above bars indicate mean CT value detected by rtPCR, and gene expression is normalized to cyclophilin A in both tissues. ****, $p \leq 0.0001$ vs. same tissue in Control ASO-treated mice; ##, $p \leq 0.01$ and ###, $p \leq 0.001$ vs. ASO-matched liver samples two-way ANOVA.

(B) Gonadal white adipose tissue weight in male mice fed chow or HFD

(C) FMO enzymatic activity (d9-TMA to d9-TMAO conversion rates) in mouse tissues. ****, $p \leq 0.0001$ vs. male mice on same diet. +, $p \leq 0.05$ vs. female mice on chow

(D) Food consumption normalized to body weight in female mice maintained on HFD or HFD with 0.02% w/w TMAO (HFD+TMAO)

(E) Plasma and (F) Liver and gonadal white adipose tissue (gWAT) TMAO levels in female mice maintained on HFD or HFD+TMAO. *, $p \leq 0.05$, **, $p \leq 0.01$, ****, $p \leq 0.0001$ vs HFD, same tissue; #, $p \leq 0.05$ and #####, $p \leq 0.0001$ vs. Control ASO mice on same diet by two-way ANOVA

Supplemental Experimental Procedures:

Human Studies:

Human Study # 1: Studies Examining Circulating Choline and TMAO Levels in Type 2 Diabetics (Related to Figure 1, Figure S1 and Supplemental Table 1). To examine whether circulating choline and TMAO levels were associated with type 2 diabetes risk, we recruited two unique cohorts with diverse cardiometabolic risk profiles. Both studies were approved by the Cleveland Clinic Institutional Review Board, and every subject provided written informed consent. For the cardiology cohort, sequential subjects (n=187) presenting to the Preventive Cardiology Clinic at the Cleveland Clinic with suspicion of fatty liver were consented and enrolled for a registry. Fasting blood was collected into EDTA vacutainer tubes, maintained on ice, and processed into plasma, and frozen at -80°C within 2 hours of collection. For the hepatology cohort, sequential subjects (n=248) presenting to the Hepatology Clinic at the Cleveland Clinic for planned diagnostic liver biopsy were consented and enrolled for a sample repository and clinical data registry. Fasting blood was collected into EDTA vacutainer tubes, maintained on ice, and processed into plasma, and frozen at -80°C within 2 hours of collection. Type 2 diabetes diagnosis was classified according to the American Diabetes Association criteria (American Diabetes Association, Diagnosis and classification of diabetes mellitus. 2016, Diabetes Care 39, Suppl 1: S54-55). Plasma levels of TMAO were quantified using the quantitative LC/MS-MS method described below and as previously published (Wang et al., 2014). Given this is the first published description of these cohorts, we provide detailed tables above with patient demographics, laboratory values, and clinical characteristics.

Human Study # 2: Large Population Adipose Tissue Microarray Cohort (Related to Figure 2E): To examine the relationship between *FMO3* expression and metabolic traits, we took advantage of a large population-based study with subcutaneous adipose biopsy as an endpoint. The *Metabolic Syndrome in Men* (METSIM) study is a cross-sectional longitudinal study that included 10,197 men, aged from 45 to 73 years randomly selected from the population of Kuopio Finland and examined in 2005-2010 (<http://www.nationalbiobanks.fi/index.php/studies2/10-metsim>). The aim of the study was to investigate genetic and non-genetic factors associated with the risk of type 2 diabetes, cardiovascular disease, and insulin resistance-related traits in a cross-sectional and longitudinal setting. A detailed description of clinical characteristic, laboratory values, and metabolic phenotyping has been published previously (Stancakova et al., 2009; Stancakova et al., 2011). Glucose tolerance was classified according to the American Diabetes Association criteria (American Diabetes Association, Diagnosis and classification of diabetes mellitus. 2016, Diabetes Care 39, Suppl 1: S54-55). and the Matsuda Index was calculated as previously described (Matsuda and DeFronzo, 1999). The study was approved by the ethics committee of the University of Eastern Finland and Kuopio University Hospital and was conducted in accordance with the Helsinki Declaration. All study participants gave written informed consent. For the data shown in Figures 2E, subcutaneous fat biopsy samples were obtained from a random sample of the participants (n = 770) of the METSIM baseline study (age 54.8 ± 5.1 years; BMI 26.6 ± 3.5 kg/m²). Total RNA was isolated from these samples using Qiagen miRNeasy Kit according to the manufacturer's instructions. RNA integrity number values were assessed with the Agilent Bioanalyzer 2100 and samples with RNA integrity number >7.0 were used for transcriptional profiling. Expression profiling using Affymetrix U219 microarray was performed at the Department of Applied Genomics Bristol-Myers Squibb according to manufacturer's protocols. The probe sequences were reannotated to remove probes that mapped to multiple locations, contained SNPs with greater than 1% MAF as assessed in 1,000 genomes European populations in their target sequences, and did not map to known transcripts based on the RefSeq (version 59) and ENSEMBL (version 72) databases. For subsequent analysis we used 43,145 probesets that represent 18,155 unique genes. The microarray image data were processed using the Affymetrix GCOS algorithm, utilizing quantile normalization or the robust multiarray (RMA) method to determine the specific hybridizing signal for each gene. Expression data can be obtained from Gene Expression Omnibus (GEO) database with the accession number GSE70353.

Study # 3: Validation Adipose Tissue Microarray Studies in Ethnically Diverse Cohorts (Related to Figure S2): Given that the large population adipose tissue microarray study (METSIM) only included Finnish men, we set out to validate mRNA expression data in several distinct cohorts spanning both men and women of European American and African American ethnicity. Importantly, both of the selected validation cohorts had extensive insulin sensitivity data evaluated by Minimal model analysis (MINMOD) of frequently sampled intravenous glucose tolerance tests (FSIVGT). The first cohort included n=99 non-Hispanic Caucasian Americans including 42 males and 57 females. All participants provided written informed

consent under protocols approved by the University of Arkansas for Medical Sciences (IRB #53028) and by the Institutional Review Board at Wake Forest School of Medicine (IRB#00011083). A detailed description of clinical characteristics, laboratory values, and metabolic phenotyping has been published previously (Das et al., 2015). The second cohort included n=260 African Americans including 139 males and 121 females. All participants provided written informed consent under protocols approved by the Institutional Review Board at Wake Forest School of Medicine (IRB#00015775). A detailed description of clinical characteristic, laboratory values, and metabolic phenotyping of this unique population has been published previously (Sharma et al., 2016). Both of these populations underwent subcutaneous adipose biopsies, with subsequent microarray analysis using the Illumina HT12-V4 expression beadchip platform (Das et al., 2011; Das et al., 2015; Sharma et al., 2016). This Illumina platform included two expressed probes for *FMO3*: ILMN_2344283 (NM_001002294.1) and ILMN_1808657 (NM_006894.4). The expression of the two *FMO3* probes were strongly correlated ($r > 0.93$, Pearson correlation coefficient), thus to evaluate the correlation of *FMO3* with other brown/beige adipocyte transcripts, we used only ILMN_2344283 (NM_001002294.1) for the comparison.

Study # 4: Human Liver Biopsy Cohort (Related to Figure S3): The purpose of this study was to examine the relationship between hepatic *FMO3* expression and metabolic phenotypes such as steatosis, hyperlipidemia, insulin sensitivity, and obesity in humans. The majority of subjects recruited here were morbidly obese bariatric surgery patients, but we were able to obtain liver biopsies from 11 subjects with a BMI under 30 as normal weight controls. For recruitment, adult patients undergoing gastric bypass surgery at Wake Forest School of Medicine provided written consent and were enrolled by a member of the study staff following institutionally approved IRB protocols. Exclusion criteria included: positive anti-hepatitis C antibody, positive hepatitis B surface antigen, or circulating hepatitis B DNA, history of liver disease other than NAFLD, Childs A, B, or C cirrhosis, past or present diagnosis/treatment of malignancy other than non-melanomatous skin cancer, INR greater than 1.8 at baseline or need for chronic anticoagulation with warfarin or heparin products, use of immunomodulation for or history of inflammatory diseases including but not limited to malignancy, rheumatoid arthritis, psoriasis, lupus, sarcoidosis and inflammatory bowel disease, and greater or equal to 7 alcohol drinks per week or 3 alcoholic drinks in a given day each week. In addition to bariatric surgery patients, a small number of non-obese subjects (body mass index < 30.0) consented to liver biopsy during elective gall bladder removal surgery (n=11). Each subject was assigned a unique identifier which was used throughout the study and did not include any identifiable information about the patient such as name, address, telephone number, social security number, medical record number or any of the identifiers outlined in the HIPAA Privacy Rule regulations. Only the principal investigator had access to the code linking the unique identifier to the study subject. Basic clinical information was obtained via self-reporting and a 15 ml baseline blood sample was obtained at the time of enrollment. A subset of this cohort has been previously described (Shores et al., 2011). At the time of surgery, a roughly 1 gram sample from the lateral left lobe was collected by the surgeon. Wedge biopsies were rinsed with saline and immediately snap frozen in liquid nitrogen in the operating room before subsequent storage at -80°C . For quantification of hepatic *FMO3* protein levels, whole liver protein lysates were made in a modified RIPA buffer as previously described (Brown et al., 2004), and protein was quantified using the BCA assay (Pierce). In order to quantify absolute amounts of hepatic *FMO3*, a protein standard curve was created using recombinant *FMO3* supersomes (Corning). Patient proteins along with recombinant protein standard curves were separated by 4–12% SDS-PAGE, transferred to polyvinylidene difluoride (PVDF) membranes, and proteins were detected after incubation with specific antibodies as previously described (Brown et al., 2004; Brown et al., 2008a; Brown et al., 2008b; Brown et al., 2010). Antibodies used for immunoblotting were anti-*FMO3* rabbit polyclonal (ABCAM #Ab126790) and anti- β actin rabbit monoclonal (Cell Signaling Technologies #4970).

Hybrid Mouse Diversity Panel (HMDP) Studies Examining the Link Between TMAO and Obesity Traits (Related to Figure 2A-2D)

92 inbred strains of 8-week-old male mice (180 individual mice) were fed a high fat and high sucrose diet (D12266B, Research Diets, New Brunswick, NJ) for 8 weeks before tissue collection (Parks et al., 2013). Plasma TMAO levels were measured and correlated with obesity-related traits using biweight midcorrelation analysis.

Mouse Studies Using Antisense Oligonucleotide (ASOs) to Knockdown the TMAO-Producing Enzyme *FMO3* (Related to Figures 3 and 4)

To study the role of the TMAO-producing enzyme FMO3 in diet-induced obesity and insulin resistance, we employed an in vivo knockdown approach in adult mice (6-8 weeks of age). Antisense oligonucleotide (ASO)-mediated knockdown was accomplished using 20-mer phosphorothioate ASOs designed to contain 2'-O-methoxyethyl groups at positions 1 to 5 and 15 to 20 as we have previously published (Warrier et al., 2015). All ASOs used in this work were synthesized, screened, and purified as described previously (Crooke et al., 2005) by Ionis Pharmaceuticals, Inc. (Carlsbad, CA). For FMO3 knockdown studies, young (6-8 week old) female C57BL/6 mice were purchased from Harlan (Indianapolis, IN, USA), and maintained on either a standard rodent chow diet or a high fat diet (45% of energy from Lard; Brown et al. 2010) and injected intraperitoneally biweekly with 25 mg/kg of either non-targeting control ASO (5'-TCCCATTTCAGGAGACCTGG-3') or an ASO directed against murine *Fmo3* (5'-TGGAAGCATTTCCTTAAA-3') for a period of 6-20 weeks, according to experimental endpoint. For magnetic resonance imaging studies (Figure 3F-3J), mice were treated with ASOs for a period of 14 weeks before imaging. For cold tolerance studies (Figure 4E), mice were treated with ASOs and maintained on a high fat diet for 5 weeks before being housed for 6 hours under room temperature (22°C) or cold condition (4°C) before necropsy under the same conditions. For indirect calorimetry studies (Figure 4F-4H), mice were treated with ASOs and fed a high fat diet for 16 weeks prior to study, and allowed to equilibrate to metabolic cage environments for ~ 48 hours before entering into 24 hour periods at thermoneutrality (30°C), room temperature (22°C), or cold temperature (4°C). Oxygen consumption (VO₂), heat, and respiratory exchange ratio (RER) were constantly monitored using the Oxymax CLAMS home cage system (Columbus Instruments). For dietary TMAO addback studies (Figure 4I-4K), female C57BL/6 mice were injected intraperitoneally with either a control ASO or *Fmo3* ASO (50 mg/kg body weight per week) for a total of 12 weeks while being maintained on the high fat diet described above, or the same diet supplemented with TMAO (0.2%, wt/wt) as previously described (Warrier et al., 2015). For experiments examining the fasting/fed transition (Figure 6D-6H), mice were treated with ASOs for 6 weeks and all sacrificed between 7:00-8:00 am (beginning of light cycle), with the fasted group having had food removed 12 hours prior at 7:00 pm. analysis. For ASO studies, all mice were maintained in an Association for the Assessment and Accreditation of Laboratory Animal Care, International-approved animal facility, and all experimental protocols were approved by the institutional animal care and use committee of the Cleveland Clinic.

Generation of FMO3 Knockout Mice Using Clustered Regularly Interspaced Short Palindromic Repeats with Cas9 Nuclease (CRISPR-Cas9) Technology (Related to Figure 5)

The target sequence (5'-GATAGGGCTACTGAAAGGGT-3') complementary to a region in exon 2 of the coding sequence of mouse *Fmo3* was used for guide RNA construction. The Cas9 mRNA and guide RNA targeting *Fmo3* were microinjected into the fertilized mouse eggs of strain C57BL/6 to generate mice that potentially carry the *Fmo3* gene mutations. DNA samples from the potential *Fmo3* mutant mice were PCR-amplified using primers located in the intron 1 (AGAGTGCTGATTGCATATGGC) and intron 2 (AGTCTCGGGCCTCCTTATCA) region of mouse *Fmo3*, generating a 493 bp PCR product. The PCR product was subjected to denaturing and reannealing, followed by cleavage by the Surveyor DNA endonuclease (Integrated DNA technologies, Coralville, Iowa) that recognizes this single-strand loop within the DNA amplicon, introducing a double-strand break at that location. Therefore, DNA samples from homozygous (wild-type or in rare cases of exact same mutant on both alleles) mice will not be cleaved, whereas those from the heterozygous mice will be cleaved into 338 bp and 155 bp DNA fragments. Seven founder mice carrying mutations in the target region of *Fmo3* were identified using this method (data not shown). We subsequently sequenced cloned PCR products of the target region of those seven to determine the nature of those mutations. Five different small in/del mutations that result in frame-shift mutation and premature termination of FMO3 protein were identified (supplemental Table 2) and further characterized (Supplemental Table 2). All FMO3 knockout animal experiments were approved by the UCLA Animal Care and Use Committee in accordance with PHS guidelines. Eight month old female wild-type (*Fmo3*^{+/+}), heterozygous (*Fmo3*^{+/-}), and homozygous (*Fmo3*^{-/-}) littermates were fed a chow diet supplemented with 1.3% choline chloride for 12 weeks before tissue collection. In a second study, *Fmo3*^{-/-} mice were crossed onto the *Ldlr*^{-/-} background to generate *Ldlr*^{-/-};*Fmo3*^{-/-} and *Ldlr*^{-/-};*Fmo3*^{+/-} littermates. Two-month-old female *Ldlr*^{-/-};*Fmo3*^{-/-} and *Ldlr*^{-/-};*Fmo3*^{+/-} mice were fed a Western diet (RD-D12079B, Research Diets, New Brunswick, NJ) for 12 weeks before tissue collection. Obesity related traits were collected as previously described (Shih et al., 2015).

Measurement of Plasma Trimethylamine and Trimethylamine-N-oxide (Related to all Figures)

Quantification of TMA and TMAO in human or mouse plasma was performed using stable isotope dilution HPLC with online electrospray ionization tandem mass spectrometry on an API 365 triple quadrupole mass spectrometer (Applied Biosystems, Foster, CA) with upgraded source (Ionics, Bolton, ON, Canada) interfaced with a Cohesive HPLC (Franklin, MA) equipped with phenyl column (4.6 × 250 mm, 5 μm Silica (2), Morton Grove, IL), and the separation was performed as reported previously (Wang et al., 2011; Wang et al., 2014). TMAO and TMA were monitored in positive MRM MS mode using characteristic precursor-product ion transitions: m/z 76 →58 and m/z 60→44, respectively. The internal standards TMAO-trimethyl-d9 (d9-TMAO) and TMA-d9 (d9-TMA) were added to plasma samples before sample processing and were similarly monitored in MRM mode at m/z 85→68 and m/z 69→49, respectively. Various concentrations of TMAO and TMA standards and a fixed amount of internal standards were spiked into control plasma to prepare the calibration curves for quantification of plasma TMAO and TMA. For d9-TMA and d9-TMAO quantification in FMO activity analyses, 1,1,2,2-d4 choline (Sigma) was used as an internal standard followed by a 0.5 ml 3K cutoff centrifugal filter (Millipore) of sample prior to LC/MS/MS analysis. The characteristic precursor-product ion transition for 1,1,2,2-d4 choline is m/z 108→60 monitored in positive MRM MS mode.

Measurement of Total Tissue Flavin Monooxygenase (FMO) Activity (Related to Supplemental Figure 3)

Determination of enzymatic activity of tissue FMOs was conducted in 250 μl reaction mix containing 1 mg tissue protein homogenate, 100 μM d9-TMA, and 100 μM reduced nicotinamide adeninedinucleotide phosphate (NADPH) in 10 mM HEPES (pH 7.4). Reaction was stopped 8 hr later with 0.2 N formic acid, followed by filtering through a 3 K cutoff spin filter, and then snap frozen and stored at -80°C until time of analysis. For analyses, internal standard was added to the thawed filtrate, which was then injected onto an HPLC column with online tandem mass spectrometer to measure the oxidized product d9-TMAO as described above. Control studies performed omitting NADPH did not show conversion of TMA into TMAO.

***In Vivo* Body Composition by MRI (Related to Figure 3F-3J)**

Relaxation-Compensated Fat Fraction (RCFF) MRI was used to provide quantitative *in vivo* assessments of subcutaneous and peritoneal adipose tissue volumes as well as lean body mass as previously described (Johnson et al., 2012). Briefly, each animal was anesthetized in 1-2% isoflurane and positioned in a 7T Bruker Biospec (Bruker Inc., Billerica, MA) MRI scanner. The respiration rate (60 +/- 20 breaths / minute) and core body temperature (35 +/- 1C) were controlled throughout the imaging experiment. The RCFF-MRI acquisition was then used to generate high-resolution coronal MRI images of the entire mouse at different echo times (Figure 3). All images were then exported for offline processing in Matlab (The Mathworks, Natick, MA). The RCFF-MRI image analysis method first generates separate fat and water images sets and then mathematically recombines these fat and water images to calculate fat fraction images [fat / (water + fat)] compensated for both T1 and T2 relaxation times. These quantitative fat fraction images provide the basis for automatic segmentation of adipose tissue (fat fraction > 0.8) from other tissues such as liver and muscle. Subsequent segmentation of the peritoneal wall calculates peritoneal and subcutaneous adipose tissue volumes as well as lean body mass for each animal using the adipose tissue volumes and the total body weight for each animal.

Immunoblotting (Related to Figure 5)

Immunoblotting experiments were performed as previously described (Shih et al., 2015). The primary antibodies against FMO3 and β-actin were purchased from Abcam, Inc. (Cambridge, MA) and Cell Signaling Technology (Danvers, MA), respectively

Real-Time PCR Analysis of Gene Expression (Related to Figures 3A, 4B, 4E, 4J, 4K, 5H, 6F-6H)

Tissue RNA extraction was performed as previously described for all mRNA analyses (Brown et al., 2008a; Brown et al., 2008b; Brown, et al., 2010; Lord et al., 2012). Quantitative real time PCR (qPCR) analyses were conducted as previously described (Brown et al., 2008a; Brown et al., 2008b; Brown, et al., 2010; Lord et al., 2011). mRNA expression levels were calculated based on the ΔΔ-CT method. qPCR was conducted using the Applied Biosystems 7500 Real-Time PCR System.

Primers used for qPCR are available on request.

Histological Analysis (Related to Figure 4A)

Hematoxylin and eosin staining of paraffin-embedded gonadal adipose sections was performed as previously described (Brown et al., 2010).

Quantification of Adipose β 1AR Density and cyclic AMP (cAMP) Levels (Related to Figure 4C, 4D)

β AR density was determined by incubating 20 μ g of the membranes (plasma membranes) with saturating concentrations of [125 I]-cyanopindolol (250 pmol/L) alone or along with 100 μ M propranolol for non-specific binding as described previously (Naga Prasad et al., 2001; Vasudevan et al., 2011). Furthermore, to distinguish between β 1AR and β 2ARs, 20 μ g of the membranes were pre-incubated with either 100 μ M metoprolol (a selective β 1AR blocker) or ICI 118,551 (a selective β 2AR blocker) followed by saturating concentrations of [125 I]-cyanopindolol. After 1 hour of incubation at 37°C, the membranes were harvested onto filters and measured for receptor density as described previously (Naga Prasad et al., 2001). Adenylyl cyclase (AC) assays were carried out by incubating 20 μ g of membranes (isolated plasma membranes or endosomes) at 37°C for 15 minutes with labeled α [32]P-ATP as previously described (Choi et al., 1997; Nienaber et al., 2003). Isoproterenol was used instead of albuterol in the plasma membranes/endosomal resensitization experiments because Isoproterenol is a full agonist, which allows for higher G-protein coupling resulting in measurable levels of in vitro cAMP generation especially in the endosomal fractions. The cAMP content was determined in the cytosol using catch point cAMP kit (Molecular Devices; Sunnyvale, CA) as per manufacturer's instruction (Vesudevan et al., 2011).

Statistical Analysis

To examine the association between circulating choline and TMAO with type 2 diabetes Wilcoxon rank-sum tests were used for continuous variables and χ^2 tests for categorical variables were used to examine the differences between participants who had diabetes events and those who did not. Logistic regression models were used to estimate odds ratio and 95% confidence interval for diabetes. All analyses were performed using R 3.1.0 (Vienna, Austria) and $p < 0.05$ was considered statistically significant. All mouse data were analyzed using either one-way or two-way analysis of variance (ANOVA) where appropriate, followed by Student's t tests for post hoc analysis. Differences were considered significant at $p < 0.05$. All mouse data analyses were performed using JMP Pro 10 (SAS Institute; Cary, NC) or Graphpad Prism 6 (La Jolla, CA) software.

Supplemental References:

Barbosa-Morais, N.L., Dunning, M.J., Samarajiwa, S.A., Darot, J.F., Ritchie, M.E., Lynch, A.G., and Tavare, S. (2010). A re-annotation pipeline for Illumina BeadArrays: improving the interpretation of gene expression data. *Nucleic Acids Res.* 38, e17.

Brown, J.M., Boysen, M.S., Chung, S., Fabiyi, O., Morrison, R.F., and McIntosh, M.K. (2004). Conjugated linoleic acid induces human adipocyte delipidation: autocrine/paracrine regulation of MEK/ERK signaling by adipocytokines. *J. Biol. Chem.* 279, 26735-26747.

Brown, J.M., Chung, S., Sawyer, J.K., Degirolamo, C., Alger, H.M., Nguyen, T., Zhu, X., Duong, M.N., Wibley, A.L., Shah, R., et al. (2008a). Inhibition of stearyl-coenzyme A desaturase 1 dissociates insulin resistance and obesity from atherosclerosis. *Circulation* 118, 1467-1475.

Brown, J.M., Bell, T.A. 3rd, Alger, H.M., Sawyer, J.K., Smith, T.L., Kelley, K., Shah, R., Wilson, M.D., Davis, M.A., Lee, R.G., et al. (2008b). Targeted depletion of hepatic ACAT2-driven cholesterol esterification reveals a non-biliary route for fecal sterol loss. *J. Biol. Chem.* 16, 10522-10534.

- Brown, J.M., Betters, J.L., Lord, C., Ma, Y., Han, X., Yang, K., Alger, H.M., Melchior, J., Sawyer, J.K., Shah, R., et al. (2010). CGI-58 knockdown in mice causes hepatic steatosis but prevents diet-induced obesity and glucose intolerance. *J. Lipid Res.* *51*, 3306-3316.
- Choi, D.J., Koch, W.J., Hunter, J.J., and Rockman, H.A. (1997). Mechanism of beta-adrenergic receptor desensitization in cardiac hypertrophy is increased beta-adrenergic receptor kinase. *J. Biol. Chem.* *272*, 17223-17229.
- Crooke, R.M., Graham, M.J., Lemonidis, K.M., Whipple, C.P., Koo, S., and Perera, R.J. (2005). An apolipoprotein B antisense oligonucleotide lowers LDL cholesterol in hyperlipidemic mice without causing hepatic steatosis. *J. Lipid Res.* *46*, 872-884.
- Das, S.K., Sharma, N.K., Hasstedt, S.J., Mondal, A.K., Ma, L., Langberg, K.A., Elbein, S.C. (2011). An integrative genomics approach identifies activation of thioredoxin / thioredoxin reductase-1-mediated oxidative stress defense pathway and inhibition of angiogenesis in obese nondiabetic human subjects. *J Clin Endocrinol Metab.* *96*, E1308-1313.
- Izem, L., and Morton, R.E. (2009). Molecular cloning of hamster lipid transfer inhibitor protein (apolipoprotein F) and regulation of its expression by hyperlipidemia. *J. Lipid Res.* *50*, 676-684.
- Johnson, D.H., Narayan, S., Wilson, D.L., Flask, C.A. (2012). Body composition analysis of obesity and hepatic steatosis in mice by relaxation compensated fat fraction (RCFF) MRI. *J. Magn. Reson. Imaging* *35*, 837-843.
- Lord, C.C., Betters, J.L., Ivanova, P.T., Milne, S.B., Myers, D.S., Madenspacher, J, Thomas, G., Chung, S., Liu, M., Davis, M.A. et al. (2012). CGI-58/ABHD5-derived signaling lipids regulate systemic inflammation and insulin action. *Diabetes* *61*, 355-363.
- Naga Prasad, S.V., Barak, L.S., Rapacciuolo, A., Caron, M.G., and Rockman, H.A. (2001). Agonist-dependent recruitment of phosphoinositide 3-kinase to the membrane by beta-adrenergic receptor kinase 1. A role in receptor sequestration. *J. Biol. Chem.* *276*, 18953-18959.
- Nienaber, J.J., Tachibana, H., Naga Prasad, S.V., Esposito, G., Wu, D., Mao, L., and Rockman, H.A. (2003). Inhibition of receptor-localized PI3K preserves cardiac beta-adrenergic receptor function and ameliorates pressure overload heart failure. *J. Clin. Invest.* *112*, 1067-1079.
- Shi, W., Oshlak, A., and Smyth, G.K. (2010). Optimizing the noise versus bias trade-off for Illumina whole genome expression BeadChips. *Nucleic Acids Res.* *38*, e204.
- Shores, N.J., Link, K., Fernandez, A., Geisinger, K.R., Davis, M.D., Nguyen, T., Sawyer, J., and Rudel, L.L. (2011). Non-contrasted computed tomography for the accurate measurement of liver steatosis in obese patients. *Dig. Dis. Sci.* *56*, 2145-2151.
- Stancakova, A., Civelek, M., Saleem, N.K., Soininen, P., Kangas, A.J., Cederberg, H., Paananen, J., Pihlajamaki, J., Bonnycastle, L.L., Morken, M.A., et al. (2012). Hyperglycemia and a common variant of GCKR are associated with the levels of eight amino acids in 9,369 Finnish men. *Diabetes* *61*, 1895-1902.
- Vasudevan, N.T., Mohan, M.L., Gupta, M.K., Hussain, A.K., and Naga Prasad, S.V. (2011). Inhibition of protein phosphatase 2A activity by PI3Kgamma regulates beta-adrenergic receptor function. *Mol. Cell* *41*, 636-648.
- Wang, Z., Levison, B.S., Hazen, J.E., Donahue, L., Li, X.M., and Hazen, S.L. (2014). Measurement of trimethylamine-N-oxide by stable isotope dilution liquid chromatography tandem mass spectrometry. *Anal. Biochem.* *15*, 35-40.